Modeling alveolar soft part sarcomagenesis in the mouse: a role for lactate in the tumor microenvironment

Matthew L. Goodwin*[1]
Huifeng Jin*[1,2]
Krystal Straessler[5]
Kyllie Smith-Fry[1,2]
Ju-Fen Zhu[1,2]
Michael J. Monument[1,2]
Allie Grossmann[3]
R. Lor Randall[1,2]
Mario R. Capecchi[4,5]
Kevin B. Jones[1,2]

[1]Department of Orthopaedics,
[2]Center for Children's Cancer Research at the Huntsman Cancer Institute,
[3]Department of Pathology,
[4]Howard Hughes Medical Institute,
[5]Department of Human Genetics,
University of Utah, Salt Lake City, Utah, 84112, U.S.A.

Contact:
Kevin B. Jones
2000 Circle of Hope Drive, Room 4263
Salt Lake City, UT 84112
Phone: 801-585-0300
Fax: 801-585-7084
E-mail: kevin.jones@hci.utah.edu

*these authors contributed equally to this work.

Running Title: Alveolar Soft Part Sarcomagenesis in the Mouse

Summary

Alveolar soft part sarcoma (ASPS), a deadly soft tissue malignancy with a predilection for adolescents and young adults, associates consistently with t(X;17) translocations that generate the fusion gene *ASPSCR1-TFE3*. We proved the oncogenic capacity of this fusion gene by driving sarcomagenesis in mice from conditional *ASPSCR1-TFE3* expression. The completely penetrant tumors were indistinguishable from human ASPS by histology and gene expression. They formed preferentially in the anatomic environment highest in lactate--the cranial vault--, expressed high levels of lactate importers, harbored abundant mitochondria, metabolized lactate as a metabolic substrate and responded to the administration of exogenous lactate with tumor cell proliferation and angiogenesis. These data demonstrate lactate's role as a potent driver of alveolar soft part sarcomagenesis.

UU IR Author Manuscript

Significance

By conditionally expressing in mice the fusion gene *ASPSCR1-TFE3* from human alveolar soft part sarcoma (ASPS), we generated a model that recapitulates the human tumor histologically and molecularly with remarkable fidelity, enabling study of the conditions supportive of tumor development. Mouse tumors demonstrated angiogenic gene expression in the frank absence of hypoxia and were restricted to the tissue compartments highest in lactate. They expressed high levels of lactate transport proteins (MCT1s), and responded to exogenous lactate with robust proliferation and angiogenesis. Such lactate metabolism in a malignancy has been previously postulated, but never before available for direct investigation in an *in vivo* tumorigenesis model. Interventions targeting lactate metabolism may provide novel therapeutic approaches for this and other malignancies.

UU IR Author Manuscript

Highlights

- The alveolar soft part sarcoma fusion *ASPSCR1-TFE3* drives tumorigenesis in mice.
- Mouse tumors from *ASPSCR1-TFE3* mimic human sarcomas by histology and transcriptome.
- Alveolar soft part sarcomas demonstrate high Hif1α and angiogenesis without hypoxia.
- Their anatomy and response to exogenous lactate suggest tumors metabolize lactate.

UU IR Author Manuscript

UU IR Author Manuscript

Introduction

Approximately one-third of all sarcomas, the cancers of connective tissue, associate with chromosomal translocations that generate fusion genes (Helman and Meltzer, 2003). Many of these fusion genes have been shown to serve as primary drivers of sarcomagenesis (Haldar et al., 2007; Keller et al., 2004; Perez-Losada et al., 2000; Straessler et al., 2013). Alveolar soft part sarcoma (ASPS), a deadly soft tissue malignancy of enigmatic origin, consistently demonstrates a t(X;17)(p11.2;q25) translocation that produces the fusion gene *ASPSCR1-TFE3* (Ladanyi et al., 2001).

ASPS presents most frequently in the adolescent or young adult limb, often metastasizes, and generally proves resistant to chemotherapy (Folpe and Deyrup, 2006). First described in 1951 (Smetana and Scott, 1951), these highly vascular tumors demonstrate characteristic histomorphology, comprised of organoid nests of polygonal tumor cells separated by fibrovascular septa with delicate capillary arcades (Folpe and Deyrup, 2006). ASPSs also demonstrate distinct, granular structures in the cytoplasm of some cells (Ladanyi et al., 2002).

Using the few available cell lines and analysis of human ASPS tumor specimens, it has been shown that the ASPSCR1-TFE3 fusion protein functions as a master regulatory transcription factor, joining a yet-to-be deciphered activation motif from ASPSCR1 to the DNA-binding domain of the TFE3 transcription factor from the MITF family (Covell et al., 2012; Kummar et al., 2013; Ladanyi et al., 2001; Stockwin et al., 2009). Although many angiogenic genes are highly upregulated in the tumors (Lazar et al., 2007; Vistica et al., 2009), few were found to be direct transcriptional targets of the fusion protein by chromatin immunoprecipitation analyses (Kobos et al., 2013). This

suggests that some other factor, possibly related to metabolism or microenvironment, enhances angiogenesis in ASPS. We exploited an *in vivo* oncogenesis model to investigate.

UU IR Author Manuscript

UU IR Author Manuscript

Results

Generation of an inducible mouse allele of ASPSCR1-TFE3

In order to characterize the fusion gene associated with ASPS and its role in sarcomagenesis, we created a novel mouse allele designed to express *ASPSCR1-TFE3* conditionally. Briefly, the *Rosa26-LSL-AT3* allele was generated by isolating the type 2 *ASPSCR1-TFE3* fusion gene transcript from total RNA obtained from a human ASPS. The complete complementary coding sequence (cDNA) was placed in the *Rosa26* locus separated from the native promoter by a stop sequence, flanked by *loxP* sites (*LSL*), that is conditionally removed via Cre-mediated recombination. The fusion gene cDNA was followed by coding sequence for the *enhanced green fluorescent protein* (*eGFP*), linked by an internal ribosomal entry site (*IRES*) to permit tandem expression of *eGFP* whenever *ASPSCR1-TFE3* was expressed (Fig.1A).

To validate the conditional character of the *LSL-AT3* allele, heterozygous E12.5 fibroblasts were harvested, dissociated, and cultured, then exposed either to vehicle control or TATCre, a protein version of Cre-recombinase with the TAT moiety from the human immunodeficiency virus that enables transport through the cell membrane and localization to the nucleus (Joshi et al., 2002; Straessler et al., 2013). After 48 hours, cells exposed to TATCre, but not control conditions, fluoresced (Fig.1B). Reverse transcriptase polymerase chain reaction (RT-PCR) also confirmed the presence of the fusion gene transcript following Cre-mediated recombination (Fig.1C).

ASPSCR1-TFE3 *expression leads to rapid, anatomically restricted tumorigenesis*

Considering possible tumorigenesis in a comparative context, mice homozygous for conditional *AT3*, as well as other mice homozygous for previously described conditional *SS18-SSX2* (synovial sarcoma) (Haldar et al., 2007) and *EWSR1-ATF1* (clear cell sarcoma) (Straessler et al., 2013) were bred to mice bearing a tamoxifen-inducible Cre-recombinase also driven from the *Rosa26* locus (Mao et al., 1999). It has been previously noted that in the absence of tamoxifen, a small portion of cells in most tissues in the mouse will undergo Cre-mediated recombination from nuclear entry of the CreER (Haldar et al., 2007; Straessler et al., 2013). We used it in this fashion as a low-prevalence, but random tissue initiator of expression.

In the comparative cohorts, *Rosa26-*$^{LSL\text{-}EWSR1\text{-}ATF1}/_{CreER}$ mice demonstrated clear cell sarcoma mimicking tumors across a broad anatomic distribution in the 3-6 month age range. *Rosa26-*$^{LSL\text{-}SS18\text{-}SSX2}/_{CreER}$ mice manifested a similar anatomic distribution of synovial sarcoma mimicking tumors, but following a longer latency of closer to a year. *Rosa26-*$^{LSL\text{-}AT3}/_{CreER}$ mice developed either unusual behavior or a visibly enlarging occiput between 3 and 6 months of age. On necropsy, every mouse was noted to have developed a tumor within the skull (Fig.2A-B).

Rosa26-$^{LSL\text{-}AT3}/_{CreER}$ mice often demonstrated enlargement of the occipital bone from inner soft tissue expansion (Fig.2C-D). Slightly pink colored tumors (Fig.2E-F) were found primarily in the brain parenchyma, but also in the choroid plexus and orbit (Fig.2.I-K). The *AT3*-induced tumors fluoresced (Fig.2G-H), indicating eGFP and therefore fusion gene expression.

Mouse tumors from* ASPSCR1-TFE3 *mimic human ASPS histopathology

We next determined whether or not the tumors induced by the conditional *AT3* allele recapitulated human ASPS histopathologically. Hematoxylin and eosin (H&E) staining of a panel of human ASPS and *Rosa26-*$^{LSL\text{-}AT3}/_{CreER}$ mouse tumors demonstrated the characteristic nests of polygonal cells with an open chromatin pattern, surrounded by neatly arcading capillary and larger vascular channels (Fig.3A-D). The species of origin for each slide was microscopically indistinguishable by an expert sarcoma-focused pathologist.

Diastase treatment of sections followed by periodic acid Schiff (dPAS) histochemical staining produces a pathognomic pattern in ASPS. In mouse tumors, dPAS demonstrated the characteristic granular deposits classically described in human ASPS (Fig.3E-F).

Many clinical labs use immunohistochemical staining against TFE3 as a surrogate marker for the fusion (Argani et al., 2003). We submitted human ASPS, *Rosa26-*$^{LSL\text{-}AT3}/_{CreER,}$ and *Rosa26-*$^{LSL\text{-}SS18\text{-}SSX2}/_{CreER}$ tumor sections to our clinical laboratory. Both human and mouse tumors associated with *ASPSCR1-TFE3* demonstrated the diagnostic, strong nuclear TFE3 staining (Fig.3G-H), whereas mouse tumors driven by *SS18-SSX2* provided the appropriate negative control (data not shown).

Tumors induced by conditional *AT3* expression in the mouse often arose in or near the leptomeninges, along sulci (Fig.3I). Some tumors showed a broad, pushing front that maintained the pia mater layer between tumor and surrounding brain parenchyma (Fig.3J). Others demonstrated more aggressive invasive growth, with

distinct extensions of tumor cells into the cerebellum, cerebrum, and the vessels of the choroid plexus (Fig.3K-M). Invasive foci were often invested with capillaries (Fig.3N), which may represent tumor-induced vessels or microvascular invasion.

The ASPSCR1-TFE3-driven mouse tumor transcriptome mimics human ASPS

In order to further validate the tumors generated by conditional AT3 expression as a model for human ASPS, we performed a series of transcriptomic analyses. Iterative alignment of gene expression profiles between mouse and human tumors from multiple series has proven fruitful in the past to identify the unique expression signature of a given tumor type (Haldar et al., 2007). Such analyses are best performed with a common control tissue as a sounding board or background for each tumor transcriptome. Because most human ASPSs arise within skeletal muscles, and high quality muscle samples could be obtained from both mice and humans, we selected skeletal muscle as our comparative control, even though it was clear that the mouse tumors did not arise from muscle.

Sequencing of cDNA libraries prepared from total RNA (RNAseq) from 5 histologically- and translocation-confirmed human ASPSs, 3 human skeletal muscle samples, 5 *Rosa26-*$^{LSL\text{-}AT3}/_{CreER}$ induced mouse tumors, and 3 mouse skeletal muscle samples yielded species-specific alignments that could be compared after filtering and re-assigning mouse genes onto human homologues. Cross species gene set enrichment analysis (GSEA) was then performed for the 500 most significantly up-regulated and 500 most significantly down-regulated genes in each intra-species tumor to muscle comparison. In both directions, GSEAs showed strong and significant

enrichment for the up-regulated gene sets (FDR q-value < 0.0005 for each GSEA) and no enrichment for the down-regulated gene sets (FDR q-value = 1.0 for all. Fig.4A). This was repeated for the 2nd through 5th groups of 500 most up-regulated genes from the human RNAseq comparison in the mouse samples, such that all genes at least two-fold significantly up-regulated were tested. All 5 of these gene sets were significantly enriched in the mouse tumor to muscle gene ranking with NES > 1.8 and FDR q-value < 0.0005 for each. Such enrichment of homologous genes suggests a strong transcriptomic match between the mouse model and human ASPS.

For an external validation, microarray-derived expression profiles on the Affymetrix Human Genome U133 Plus 2.0 Array from 7 human ASPSs and 5 human skeletal muscle control samples were obtained from the Gene Expression Omnibus (GEO) records GSE13433 and GSE34111. Each list of up-regulated genes was significantly enriched by GSEA in comparison across species and RNAseq versus microarray platforms (FDR q-value < 0.0005 for each). Each list of down-regulated genes showed no enrichment (FDR q-value = 1.0 for each. Fig.4A). As a second external validation, we evaluated the expression of the 51 human genes found by Kobos et al. to be upregulated in multiple human series and whose promoters were found to be bound by the fusion oncoprotein in chromatin immunoprecipitation experiments. 45 of these genes were at least 1.5-fold up-regulated in mouse tumors compared to mouse muscles.

In order to determine a species transcendent *ASPSCR1-TFE3* gene expression signature, we identified all human genes or mouse homologues that were at least 2-fold up-regulated and statistically significant ($p < 0.05$) in all three tumor to muscle

UU IR Author Manuscript

comparisons (Supplemental Table 1). A heatmap of these 539 unique genes, contrasting log2 transformed fold-changes of tumors versus controls (Fig.4B) showed consistently high expression across individual tumors samples from each group. Finally, assessment of the character of these consistently up-regulated genes by GO-Elite analysis noted carbohydrate metabolism, cell division, and cell cycle as the most significant biological process gene ontologies (Fig.4C).

ASPSCR1-TFE3 ***expression leads to spatially restricted tumorigenesis even among different cell lineages***

The observation that tumors in *Rosa26-*$^{LSL\text{-}AT3}/_{CreER}$ mice recapitulated human ASPS features so clearly by histopathology and transcriptomic analysis only enhanced our notice of the striking difference between the two species in anatomic distribution. Whereas most human ASPSs arise in skeletal muscle, none of the *Rosa26-*$^{LSL\text{-}AT3}/_{CreER}$ mice developed tumors in the skeletal muscle. This contrasted with our comparison mouse genetic cancer models which actually favored development of tumors within skeletal muscles, despite expressing their respective fusion genes from the identical locus and initiated by the same driver of Cre-recombinase (Fig.2B).

Suspecting that the mouse brain might harbor some preferred cell of origin for transformation by *AT3* expression, leading to tumorigenesis that was too rapid to allow slower limb tumors to become detectable, we next crossed mice bearing conditional *AT3* with mice bearing a lineage-restricted tamoxifen-inducible Cre-recombinase, expressed from a *Prx1* promoter (*Prx1-CreERT2*) (Hasson et al., 2007). *Prx1-CreERT2* mice have a well-documented lineage that emphasizes osteochondral progenitors in the

UU IR Author Manuscript

periosteal mesenchyme, but also includes some intramuscular pericytes (Kawanami et al., 2009; Logan et al., 2002; Straessler et al., 2013). *Prx1-CreERT2;Rosa26*$^{LSL\text{-}AT3}$/$_{wt}$ mice consistently developed intracranial tumors 10-14 weeks after tamoxifen at age 2 weeks. Interestingly, tumors were located either within the brain parenchyma or in the periosteum along the inner table of the cranium (Fig.5A). No tumors were identified in the outer table periosteum or the limbs, where most of the post-natal *Prx1* lineage is found.

Prx1 expression in neural stem cells has been previously described (Shimozaki et al., 2013). We have also previously shown the lineage to include perivascular mesenchymal cells (Straessler et al., 2013). Either of these portions of the *Prx1* lineage might explain the intra-parenchymal tumors, but the periosteal tumors presented a conundrum. First, these periosteal cells of origin were decidedly not within the brain parenchyma, ruling out our initial suspicion of a preferred cell of origin in that host tissue. Second, the periosteal lineage (including mesenchymal progenitors to both osteochondral and endothelial differentiation) should not be different morphologically on the inner surface of the cranium than outside the cranium.

To compare the presence of the lineage on the inner table of the cranial periosteum, we crossed *Prx1-CreERT2* bearing mice to mice bearing a *Rosa26-LSL-LacZ* reporter allele (Soriano, 1999). X-gal staining of 3 week old *Prx1CreERT2;Rosa26*$^{LSL\text{-}LacZ}$/$_{wt}$ mouse brains post receipt of tamoxifen at 2 weeks demonstrated periosteal staining along the inner and outer tables of the cranium as well as in the limb periosteum (Fig.5B).

UU IR Author Manuscript

Notably, the extra-cranial periosteum stained just as consistently as did the intra-cranial periosteum with lineage tracing, but only the latter gave rise to tumors in *Prx1CreERT2;Rosa26*$^{LSL\text{-}AT3}$/$_{wt}$ mice. The spatially restricted development of periosteal tumors intra- but not extra-cranially suggested that something unique to the microenvironment inside the cranial vault enhanced at least the efficiency of tumorigenesis there.

ASPSCR1-TFE3 ***tumors are primed to import lactate***

To triangulate our thinking about the microenvironment pertinent to intracranial mouse tumors and human ASPSs in skeletal muscle, we returned to what both species' tumors had in common: deranged carbohydrate metabolism (Fig.4C). Both brain and muscle have been the primary tissues of focus in the elucidation over recent decades of the phenomenon termed lactate flux (Brooks and Gaesser, 1980; Gladden, 2008). Some cells either temporarily or consistently export lactate produced by glycolysis. Other cells (in nearby or distant tissues accessed through the circulation) import and metabolize that lactate. While muscle can demonstrate a high volume lactate flux during activity, the brain consistently moves lactate between cells via the astrocyte-neuron shuttle (Aubert et al., 2005).

Significant lactate import requires elevated interstitial or intravascular lactate and the expression of monocarboxylate transporters (MCTs). Although lactate can cross membranes via other means, MCTs are responsible for the bulk of lactate transport. MCT1 and its binding partner CD147 are highly expressed in tissues that primarily

UU IR Author Manuscript

import lactate; MCT4 is highly expressed in tissues that primarily export lactate (Halestrap, 2013).

We assessed the raw RNAseq expression levels (in fragments per kilobase of exon per million fragments mapped, or FPKM units) of monocarboxylate transport genes in tumors and muscles. The muscle provided an ideal comparison control tissue, as skeletal muscle is known to express high levels of lactate transport genes. The two genes comprising the lactate transport complex associated with lactate importation, *Mct1* and *Cd147*, were very highly over-expressed in tumors compared to muscles or compared to any other monocarboxylate transport genes in the tumors (Fig.6A). This fit the previously reported immunohistochemical finding of these two proteins in the cytoplasmic crystals stained by dPAS in human ASPS (Ladanyi et al., 2002). Further, *Mct4*, the transport gene associated with lactate exportation, was not only expressed at a much lower level in tumors than the import-associated complex, but also at a significantly lower FPKM than in muscle.

MCTs are not pumps; their function requires lactate available for import. We therefore biochemically measured the lactate concentration in a panel of tissues in normal 2 month-old mice. Brain and eye, the host tissue compartments of all the AT3-driven tumors, demonstrated the highest tissue lactate concentrations (Fig.6B).

Lactate serves as a metabolic substrate in ASPSCR1-TFE3 *tumors*

In order for imported lactate to contribute to metabolism, the cell would have to have significant oxidative capacity. As a measure of the abundance of mitochondria, we examined the expression of genes coding for proteins confirmed to locate within

UU IR Author Manuscript

mitochondria, using the Broad Institute's MitoCarta list. Again, the comparison control of muscle was fortuitous in that muscle exhibits one of the highest mitochondrial contents in normal mammalian tissues. Surprisingly, ASPSCR1-TFE3-driven tumors demonstrated dramatic up-regulation of nearly the entire complement of mitochondrial genes compared to quadriceps muscle controls, in both mouse and human comparisons (Fig.7A-B).

We also measured the oxygen consumption of fresh tissue sections from AT3-driven mouse tumors compared to other tumor controls, both at baseline in minimal media and following administration of lactate substrate. ASPSCR1-TFE3-driven mouse tumors were more oxidative than comparison mouse tumor types at baseline and responded oxidatively to the administration of lactate substrate (Fig.7C-D).

Lactate serves as a signaling molecule in ASPSCR1-TFE3 *tumors*

While considered to be induced by hypoxia through down-regulation of its hydroxylation and proteosomal degradation at low oxygen levels, HIF1α also directly responds to lactate levels within a cell (Fig.8A) (Burns and Wilson, 2003; Kumar et al., 2007; Xiong et al., 1998). Needless to say, this phenomenon contributes to the hypoxic stabilization of HIF1α, as intracellular lactate accumulates in hypoxia, but does not strictly require hypoxia itself.

It has been previously shown that human ASPS has high levels of HIF1α (Kenney et al., 2011; Stockwin et al., 2009; Vistica et al., 2009). If these levels were generated in response to imported lactate, as opposed to lactate produced within the cell, they should be independent of hypoxia. We quantitated the level of hypoxia within

the tumors by administering pimonidazole to tumor-bearing *Rosa26-*$^{LSL\text{-}AT3}$*/*$_{CreER}$ mice prior to euthanasia. Only in the presence of hypoxia (oxygen tensions lower than 10 torr) will pimonidazole form adducts with thiol groups that are detectable by immunohistochemistry with an available monoclonal antibody (Rosenberger et al., 2009).

Control tissues of the kidney, liver, brain, and skin were collected as well as tumors from each mouse. While the normal prevalence of pimonidazole adducts and therefore hypoxia was detected in each of the control tissues, few tumors demonstrated any hypoxia (Fig.8B). Tumors demonstrated less hypoxia than even the surrounding normal brain parenchyma.

Normal tissues showed demonstrable Hif1α immunohistochemistry only in hypoxic regions, such as the renal tubules. In contrast, tumors demonstrated strong nuclear Hif1α staining throughout (Fig.8B), despite normoxia. Signaling from imported lactate can increase levels of Hif1α in normoxia. We further tested these thoroughly non-hypoxic tumors for expression of a “hypoxic” gene signature and found them to demonstrate enrichment (Fig.8C), possibly reflecting other indirectly lactate-responsive genes.

In order to test the hypothesis that *ASPSCR1-TFE3* tumors receive signaling from imported lactate, we administered lactate or saline by daily isotonic intraperitoneal (IP) injections for two weeks prior to sacrifice in a subset of mice that had developed tumors. Exogenous lactate drove dramatic increases in proliferative index and vascular density (Fig.8D-F). As cross-validation of this effect, we cultured the only two described human cancer cell lines that express *ASPSCR1-TFE3*, FU-UR-1 (Ishiguro et al., 2004;

UU IR Author Manuscript

Kobos et al., 2013) and ASPS-1 (Kenney et al., 2011) in increasing concentrations of sodium lactate, identifying a proliferative response. We further confirmed that increased exogenous lactate concentration in normoxia drove higher HIF1α stabilization, evidenced by its increased nuclear presence. This effect was blocked by tandem application of α-cyano-4-hydroxycinnamate (CHC), a chemical inhibitor of MCT1.

UU IR Author Manuscript

Discussion

We report a genetic model of alveolar soft part sarcomagenesis and have validated its mimicry of human tumors with both histologic and transcriptomic analyses. This model revealed a very unusual anatomic distribution, which has implications with regard to cell of origin and the metabolic microenvironment. Despite the already reported high expression of Hif1α and pro-angiogenic genes in ASPS, we demonstrated that these tumors lack frank hypoxia. When provided exogenous administration of lactate, the tumors responded with enhanced proliferation and dramatic angiogenesis, suggesting that lactate, not hypoxia, contributes to this unique form of sarcomagenesis.

Alveolar soft part sarcomagenesis is driven by its translocation-generated fusion oncogene

Previously, members of our group have demonstrated the oncogenicity of the fusion genes that derive from chromosomal translocations in alveolar rhabdomysarcoma (*PAX3-FKHR*) (Keller et al., 2004), synovial sarcoma (*SS18-SSX2*) (Haldar et al., 2007), and clear cell sarcoma (*EWSR1-ATF1*) (Straessler et al., 2013). Others have shown a similar transformation in the mouse by the *FUS-CHOP* fusion oncogene associated with myxoid liposarcoma (Perez-Losada et al., 2000). By using a Cre/loxP conditional construct in the *Rosa26* locus to drive expression of *ASPSCR1-TFE3*, we have now shown this fusion gene to be sufficient for completely penetrant oncogenesis in the mouse.

Remarkably, the *AT3*-driven mouse tumors were histopathologically well matched to human ASPS, demonstrating the prototypical, classic features (Fig.3).

UU IR Author Manuscript

Expression profiles were also stridently parallel between mouse and human tumors. Such interspecies comparisons have been fraught with difficulty in the past. We have previously utilized RNAseq as a less platform-constrained means of understanding the transcriptome of mouse tumor models (Straessler et al., 2013), but never before had human tumor RNAseq data for comparison, as we had in these analyses. In addition to our primary data, we also incorporated a prior microarray-based study of human ASPS gene expression and another chromatin immunoprecipitation analysis to further validate our primary RNAseq results.

Taken together, these results from both gene expression and histopathology argue that in a manner similar to synovial sarcoma and clear cell sarcoma, the complicated biology of ASPS initiation is recapitulated by mere expression of its fusion gene *ASPSCR1-TFE3*. Importantly, none of these genetic mouse models driven by expression of translocation-generated fusion oncogenes fully recapitulates the most advanced clinical stages of its related human sarcoma. In addition to the lack of overt metastases, shared by all of the above models, this ASPS model also lacks histologically clear vascular invasion, which is commonly identified in the human counterpart. However, the intra-cranial location of the tumors in our model somewhat complicates this analysis. Possibly, such aggressive features of disease require more time or larger tumor size than can be endured by mice. Notably, this emphasizes that the biology modeled is that of sarcoma initiation rather than advanced clinical disease.

UU IR Author Manuscript

Alveolar soft part sarcomagenesis is anatomically restricted in humans and mice

While the cell of origin of this unique tumor has long been controversial, our studies lend some new insights to the debate. Prior arguments have typically centered on either a myogenic or neural cell of origin, depending on gene expression in tumors as evidence of histogenesis. The formation of mouse tumors in intra-cranial tissue compartments that completely lack skeletal muscle removes the possibility of an exclusively skeletal muscle cell of origin. Of course, the same can be deduced from the human ASPSs described to have arisen primarily within the cranial vault (Bodi et al., 2009; Das et al., 2012) or cardiac muscle (Luo et al., 2008). Instead of confirming either muscle or neural origins, our experiments with the *Prx1* lineage argue that some mesenchymal progenitor, possibly pericyte/endothelial in character, provides one potential cell of origin distinct from either previously considered lineage. Because pericytes are ubiquitous throughout the body, the specific locations of tumors could not be explained by the availability of a cell of origin alone. However, a pericyte cell of origin in humans could explain the occasional ASPS tumor reported to arise in an unusual anatomic location.

We interpret the anatomic location of mouse tumors induced by expression of *ASPSCR1-TFE3* as circumstantial evidence of a preference for high environmental lactate. While this predilection for origin within the brain in the mouse is not recapitulated in human ASPSs, all the tissues which play common host to human ASPS are also thought to be high lactate tissues, such as skeletal muscle, cardiac muscle, and brain. Most human ASPSs arise in the skeletal muscle of active adolescents and young adults, a host tissue with very high lactate shuttling. Among all sarcomas, ASPS

UU IR Author Manuscript

is the most frequently (per its low prevalence) either metastatic or primary to the brain (Fox et al., 2009). While the prevalence of ASPS comprises about 1 percent of all sarcomas, it is the most common among primary or metastatic cardiac sarcomas in clinical series as well (Agaimy et al., 2012; Kumar et al., 2011). Interestingly, evidence from different experimental approaches has shown that the heart can get up to 60 percent of its energy from lactate oxidation (Gertz et al., 1988; Gladden, 2008; Stanley, 1991). While ASPS is not strictly considered to arise in the kidney--another high lactate tissue--a special subset of renal cell carcinomas express and are thought to be driven by the *ASPSCR1-TFE3* fusion gene and other TFE3 fusions (Argani et al., 2001). Much of ASPS biology has actually been inferred from studies in a clear cell carcinoma cell line that expresses *ASPSCR1-TFE3* (Ishiguro et al., 2004).

Some other information can be gleaned regarding lactate in the microenvironment from prior attempts to directly xenograft human ASPSs into the subcutaneous flanks of immnocompromised mice. Attempts with 12 different tumors yielded four successes at a latency of 8-9 months; three of those successes derived from lung or lymph node metastases (Vistica et al., 2009). While these data argue that ASPS *can* grow in host tissues lacking overtly high lactate, growth may be less efficient in those settings and may only be possible in select subclones.

Lactate uptake without hypoxia up-regulates Hif1a and angiogenesis in ASPS

Others have shown that lactate can contribute to angiogenesis (Semenza, 2008; Sonveaux et al., 2008). In glycolytic glioma tumor cells *in vitro*, lactate exposure increased HIF1α levels independent of hypoxia by inhibiting HIF1α proline

UU IR Author Manuscript

hydroxylation, leading to increased VEGF production (Lowry et al., 1983; Lu et al., 2005; Lu et al., 2002). Others have shown that oxidative tumor cells *in vitro* activate HIF1α via importation of lactate (De Saedeleer et al., 2012). IP lactate administration in mice has enhanced xenografted tumor metastasis and vascularity (Bonuccelli et al., 2010).

ASPS has long been known to be highly vascular and to express many angiogenic factors, such as HIF1α (Lazar et al., 2007; Vistica et al., 2009). We have now added to that observation the confirmation that ASPS is also normoxic. ASPSs express high levels of lactate transporters that associate with lactate import (*Mct1* and *Cd147*) but not export (*Mct4*) and have abundant mitochondria. Not only do tumors form in areas of high lactate flux both in our model and in humans, but providing exogenous lactate also dramatically increased angiogenesis and tumor cell proliferation. Human cell lines known to express *ASPSCR1-TFE3* proliferated in response to exogenous lactate and increased in nuclear HIF1α.

Several cancer metabolism investigations have emphasized the poor prognostic impact of hypoxia and high lactate, but these also typically associate with transitions to more metabolically quiescent cellular states (Brizel et al., 2001; Walenta et al., 1997; Walenta et al., 2004). This is not so with ASPS, which oxidatively metabolizes lactate and increases proliferation in response to exogenous lactate.

For years, scientists have understood HIF1α to be induced by hypoxia (Semenza, 2012). In a similar light, lactate was also long-considered to be elevated only in hypoxia. Both paradigms are shifting. There is an abundance of evidence that suggests that lactate is the primary intermediate in whole body metabolism, as is best

UU IR Author Manuscript

described by the lactate shuttle (Brooks, 2002). Further, *in vitro* studies within the last year have shown lactate to be a powerful driver of HIF1α induction in normoxic conditions (De Saedeleer et al., 2012). We were able to test directly for the first time the degree to which increasing lactate in normoxia is an angiogenic signaling molecule driving tumorigenesis *in vivo*.

To conclude, ASPS is a deadly and rare tumor that portends a poor prognosis. In our efforts to characterize this particular tumor and open the door for novel metabolic treatments, we have shown that the tumor microenvironment can have dramatic implications on tumor formation and angiogenesis, specifically in regard to the role of lactate.

UU IR Author Manuscript

Experimental Procedures

Mice

All mouse work was performed with the approval of the institutional animal care and use committee and in accordance with international legal and ethical norms. The *EWSR1-ATF1*, *SS18-SSX2*, and *LacZ* mice were previously described (Haldar et al., 2007; Soriano, 1999; Straessler et al., 2013), as were *Rosa26-CreER* and *Prx1-CreERT2* mice (Badea et al., 2003; Hasson et al., 2007). The full length cDNA of type 2 *ASPSCR1-TFE3* was reverse transcribed from total RNA isolated from a human ASPS. The *Rosa26-LSL-AT3* targeting vector was electroporated into R1 mouse embryonic stem cells, which were selected, screened, and microinjected into blastocysts. Please see the Supplemental Experimental Procedures for additional details.

Clinical

With the approval of the institutional review board and in accordance with all international legal and ethical standards, fresh surgical specimens from consenting patients were banked and stored, then analyzed after annotation with histopathological, molecular, and clinical data. Please see the Supplemental Experimental Procedures for additional details.

Transcriptome analysis

Sequencing was performed on an Illumina HiSeq 2000 (Illumina) using a 50 cycle single end read after mRNA capture by the Ribo-Zero method. The

OverdispersedRegionScanSeqs script in the USeq package (Nix et al., 2008) calculated the expression levels of ENSEMBL genes in FPKM values. USeq also discovers differentially expressed genes between two RNA-seq libraries by calling the DESeq R package (Anders and Huber, 2010).

GEO data were normalized by DChip (Li and Hung Wong, 2001). GSEA was performed with Broad Institute software (Mootha et al., 2003; Subramanian et al., 2005). The Harris hypoxia gene set is curated by the Broad Institute (Harris, 2002), as is MitoCarta, including the original 1098 mouse genes, whose proteins localize to the mitochondria, and their 1013 human homologues (Pagliarini et al., 2008). Gene ontology analysis was performed with GO-Elite software (Zambon et al., 2012). Please see the Supplemental Experimental Procedures for additional details.

UU IR Author Manuscript

Acknowledgements

The authors thank L. Bruce Gladden from Auburn University, Maarten W. N. Nijsten from University Medical Center Groningen, The Netherlands, and Don Ayer from the Department of Oncologic Sciences for helpful conversations regarding lactate physiology and metabolism, Marc Ladanyi from Memorial Sloan Kettering Cancer Center for provision of human cell lines, Matt Hockin of the Department of Human Genetics for provision of the TATCre, Sheryl Tripp from ARUP laboratories for help with immunohistochemistry, Shaobo Pei and Sihem Boudina from the metabolic phenotyping core facility for help with SeaHorse experiments, Brian Dally from the sequencing core facility for help with the RNAseq, and Tim Mosbruger and Brett Milash from the bioinformatics core facility for help with the RNAseq analysis. This work was directly supported by the Alex's Lemonade Stand Foundation (K.B.J.) and the Sherman Coleman Resident Research Award (M.L.G.). K.B.J. receives additional career development support from the Damon Runyon Cancer Research Foundation and National Cancer Institute (National Institutes of Health, NIH) K08CA138764. This work was also partly supported by P30CA042014 from the National Cancer Institute. The content is solely the responsibility of the authors and does not necessarily represent the official views of the National Cancer Institute or the National Institutes of Health.

UU IR Author Manuscript

References

Agaimy, A., Rosch, J., Weyand, M., and Strecker, T. (2012). Primary and metastatic cardiac sarcomas: a 12-year experience at a German heart center. Int J Clin Exp Pathol *5*, 928-938.

Anders, S., and Huber, W. (2010). Differential expression analysis for sequence count data. Genome Biol *11*, R106.

Argani, P., Antonescu, C.R., Illei, P.B., Lui, M.Y., Timmons, C.F., Newbury, R., Reuter, V.E., Garvin, A.J., Perez-Atayde, A.R., Fletcher, J.A.*, et al.* (2001). Primary renal neoplasms with the ASPL-TFE3 gene fusion of alveolar soft part sarcoma: a distinctive tumor entity previously included among renal cell carcinomas of children and adolescents. Am J Pathol *159*, 179-192.

Argani, P., Lal, P., Hutchinson, B., Lui, M.Y., Reuter, V.E., and Ladanyi, M. (2003). Aberrant nuclear immunoreactivity for TFE3 in neoplasms with TFE3 gene fusions: a sensitive and specific immunohistochemical assay. The American journal of surgical pathology *27*, 750-761.

Aubert, A., Costalat, R., Magistretti, P.J., and Pellerin, L. (2005). Brain lactate kinetics: Modeling evidence for neuronal lactate uptake upon activation. Proc Natl Acad Sci U S A *102*, 16448-16453.

Badea, T.C., Wang, Y., and Nathans, J. (2003). A noninvasive genetic/pharmacologic strategy for visualizing cell morphology and clonal relationships in the mouse. J Neurosci *23*, 2314-2322.

UU IR Author Manuscript

Bodi, I., Gonzalez, D., Epaliyange, P., Gullan, R., and Fisher, C. (2009). Meningeal alveolar soft part sarcoma confirmed by characteristic ASPCR1-TFE3 fusion. Neuropathology *29*, 460-465.

Bonuccelli, G., Tsirigos, A., Whitaker-Menezes, D., Pavlides, S., Pestell, R.G., Chiavarina, B., Frank, P.G., Flomenberg, N., Howell, A., Martinez-Outschoorn, U.E.*, et al.* (2010). Ketones and lactate "fuel" tumor growth and metastasis: Evidence that epithelial cancer cells use oxidative mitochondrial metabolism. Cell Cycle *9*, 3506-3514.

Brizel, D.M., Schroeder, T., Scher, R.L., Walenta, S., Clough, R.W., Dewhirst, M.W., and Mueller-Klieser, W. (2001). Elevated tumor lactate concentrations predict for an increased risk of metastases in head-and-neck cancer. Int J Radiat Oncol Biol Phys *51*, 349-353.

Brooks, G.A. (2002). Lactate shuttles in nature. Biochem Soc Trans *30*, 258-264.

Brooks, G.A., and Gaesser, G.A. (1980). End points of lactate and glucose metabolism after exhausting exercise. J Appl Physiol Respir Environ Exerc Physiol *49*, 1057-1069.

Burns, P.A., and Wilson, D.J. (2003). Angiogenesis mediated by metabolites is dependent on vascular endothelial growth factor (VEGF). Angiogenesis *6*, 73-77.

Covell, D.G., Wallqvist, A., Kenney, S., and Vistica, D.T. (2012). Bioinformatic analysis of patient-derived ASPS gene expressions and ASPL-TFE3 fusion transcript levels identify potential therapeutic targets. PLoS One *7*, e48023.

Das, K.K., Singh, R.K., Jaiswal, S., Agrawal, V., Jaiswal, A.K., and Behari, S. (2012). Alveolar soft part sarcoma of the frontal calvarium and adjacent frontal lobe. J Pediatr Neurosci *7*, 36-39.

De Saedeleer, C.J., Copetti, T., Porporato, P.E., Verrax, J., Feron, O., and Sonveaux, P. (2012). Lactate activates HIF-1 in oxidative but not in Warburg-phenotype human tumor cells. PLoS One *7*, e46571.

Folpe, A.L., and Deyrup, A.T. (2006). Alveolar soft-part sarcoma: a review and update. J Clin Pathol *59*, 1127-1132.

Fox, B.D., Patel, A., Suki, D., and Rao, G. (2009). Surgical management of metastatic sarcoma to the brain. J Neurosurg *110*, 181-186.

Gertz, E.W., Wisneski, J.A., Stanley, W.C., and Neese, R.A. (1988). Myocardial substrate utilization during exercise in humans. Dual carbon-labeled carbohydrate isotope experiments. The Journal of clinical investigation *82*, 2017-2025.

Gladden, L.B. (2008). A lactatic perspective on metabolism. Med Sci Sports Exerc *40*, 477-485.

Haldar, M., Hancock, J.D., Coffin, C.M., Lessnick, S.L., and Capecchi, M.R. (2007). A conditional mouse model of synovial sarcoma: insights into a myogenic origin. Cancer Cell *11*, 375-388.

Halestrap, A.P. (2013). The SLC16 gene family - structure, role and regulation in health and disease. Mol Aspects Med *34*, 337-349.

UU IR Author Manuscript

Harris, A.L. (2002). Hypoxia--a key regulatory factor in tumour growth. Nat Rev Cancer *2*, 38-47.

Hasson, P., Del Buono, J., and Logan, M.P. (2007). Tbx5 is dispensable for forelimb outgrowth. Development *134*, 85-92.

Helman, L.J., and Meltzer, P. (2003). Mechanisms of sarcoma development. Nat Rev Cancer *3*, 685-694.

Ishiguro, M., Iwasaki, H., Ohjimi, Y., and Kaneko, Y. (2004). Establishment and characterization of a renal cell carcinoma cell line (FU-UR-1) with the reciprocal ASPL-TFE3 fusion transcript. Oncology reports *11*, 1169-1175.

Joshi, S.K., Hashimoto, K., and Koni, P.A. (2002). Induced DNA recombination by Cre recombinase protein transduction. Genesis *33*, 48-54.

Kawanami, A., Matsushita, T., Chan, Y.Y., and Murakami, S. (2009). Mice expressing GFP and CreER in osteochondro progenitor cells in the periosteum. Biochem Biophys Res Commun *386*, 477-482.

Keller, C., Arenkiel, B.R., Coffin, C.M., El-Bardeesy, N., DePinho, R.A., and Capecchi, M.R. (2004). Alveolar rhabdomyosarcomas in conditional Pax3:Fkhr mice: cooperativity of Ink4a/ARF and Trp53 loss of function. Genes Dev *18*, 2614-2626.

Kenney, S., Vistica, D.T., Stockwin, L.H., Burkett, S., Hollingshead, M.G., Borgel, S.D., Butcher, D.O., Schrump, D.S., and Shoemaker, R.H. (2011). ASPS-1, a novel cell line

manifesting key features of alveolar soft part sarcoma. Journal of pediatric hematology/oncology *33*, 360-368.

Kobos, R., Nagai, M., Tsuda, M., Merl, M.Y., Saito, T., Lae, M., Mo, Q., Olshen, A., Lianoglou, S., Leslie, C.*, et al.* (2013). Combining integrated genomics and functional genomics to dissect the biology of a cancer-associated, aberrant transcription factor, the ASPSCR1-TFE3 fusion oncoprotein. The Journal of pathology *229*, 743-754.

Kumar, N., Agarwal, S., Ahuja, A., Das, P., Airon, B., and Ray, R. (2011). Spectrum of cardiac tumors excluding myxoma: Experience of a tertiary center with review of the literature. Pathol Res Pract *207*, 769-774.

Kumar, V.B., Viji, R.I., Kiran, M.S., and Sudhakaran, P.R. (2007). Endothelial cell response to lactate: implication of PAR modification of VEGF. J Cell Physiol *211*, 477-485.

Kummar, S., Allen, D., Monks, A., Polley, E.C., Hose, C.D., Ivy, S.P., Turkbey, I.B., Lawrence, S., Kinders, R.J., Choyke, P.*, et al.* (2013). Cediranib for metastatic alveolar soft part sarcoma. J Clin Oncol *31*, 2296-2302.

Ladanyi, M., Antonescu, C.R., Drobnjak, M., Baren, A., Lui, M.Y., Golde, D.W., and Cordon-Cardo, C. (2002). The precrystalline cytoplasmic granules of alveolar soft part sarcoma contain monocarboxylate transporter 1 and CD147. Am J Pathol *160*, 1215-1221.

Ladanyi, M., Lui, M.Y., Antonescu, C.R., Krause-Boehm, A., Meindl, A., Argani, P., Healey, J.H., Ueda, T., Yoshikawa, H., Meloni-Ehrig, A.*, et al.* (2001). The

UU IR Author Manuscript

der(17)t(X;17)(p11;q25) of human alveolar soft part sarcoma fuses the TFE3 transcription factor gene to ASPL, a novel gene at 17q25. Oncogene *20*, 48-57.

Lazar, A.J., Das, P., Tuvin, D., Korchin, B., Zhu, Q., Jin, Z., Warneke, C.L., Zhang, P.S., Hernandez, V., Lopez-Terrada, D.*, et al.* (2007). Angiogenesis-promoting gene patterns in alveolar soft part sarcoma. Clinical cancer research : an official journal of the American Association for Cancer Research *13*, 7314-7321.

Li, C., and Hung Wong, W. (2001). Model-based analysis of oligonucleotide arrays: model validation, design issues and standard error application. Genome Biol *2*, RESEARCH0032.

Logan, M., Martin, J.F., Nagy, A., Lobe, C., Olson, E.N., and Tabin, C.J. (2002). Expression of Cre Recombinase in the developing mouse limb bud driven by a Prxl enhancer. Genesis *33*, 77-80.

Lowry, O.H., Berger, S.J., Carter, J.G., Chi, M.M., Manchester, J.K., Knor, J., and Pusateri, M.E. (1983). Diversity of metabolic patterns in human brain tumors: enzymes of energy metabolism and related metabolites and cofactors. J Neurochem *41*, 994-1010.

Lu, H., Dalgard, C.L., Mohyeldin, A., McFate, T., Tait, A.S., and Verma, A. (2005). Reversible inactivation of HIF-1 prolyl hydroxylases allows cell metabolism to control basal HIF-1. J Biol Chem *280*, 41928-41939.

UU IR Author Manuscript

Lu, H., Forbes, R.A., and Verma, A. (2002). Hypoxia-inducible factor 1 activation by aerobic glycolysis implicates the Warburg effect in carcinogenesis. J Biol Chem *277*, 23111-23115.

Luo, J., Melnick, S., Rossi, A., Burke, R.P., Pfeifer, J.D., and Dehner, L.P. (2008). Primary cardiac alveolar soft part sarcoma. A report of the first observed case with molecular diagnostics corroboration. Pediatr Dev Pathol *11*, 142-147.

Mao, X., Fujiwara, Y., and Orkin, S.H. (1999). Improved reporter strain for monitoring Cre recombinase-mediated DNA excisions in mice. Proc Natl Acad Sci U S A *96*, 5037-5042.

Mootha, V.K., Lindgren, C.M., Eriksson, K.F., Subramanian, A., Sihag, S., Lehar, J., Puigserver, P., Carlsson, E., Ridderstrale, M., Laurila, E.*, et al.* (2003). PGC-1alpha-responsive genes involved in oxidative phosphorylation are coordinately downregulated in human diabetes. Nat Genet *34*, 267-273.

Nix, D.A., Courdy, S.J., and Boucher, K.M. (2008). Empirical methods for controlling false positives and estimating confidence in ChIP-Seq peaks. BMC Bioinformatics *9*, 523.

Pagliarini, D.J., Calvo, S.E., Chang, B., Sheth, S.A., Vafai, S.B., Ong, S.E., Walford, G.A., Sugiana, C., Boneh, A., Chen, W.K.*, et al.* (2008). A mitochondrial protein compendium elucidates complex I disease biology. Cell *134*, 112-123.

Perez-Losada, J., Pintado, B., Gutierrez-Adan, A., Flores, T., Banares-Gonzalez, B., del Campo, J.C., Martin-Martin, J.F., Battaner, E., and Sanchez-Garcia, I. (2000). The

chimeric FUS/TLS-CHOP fusion protein specifically induces liposarcomas in transgenic mice. Oncogene *19*, 2413-2422.

Rosenberger, C., Rosen, S., Paliege, A., and Heyman, S.N. (2009). Pimonidazole adduct immunohistochemistry in the rat kidney: detection of tissue hypoxia. Methods Mol Biol *466*, 161-174.

Semenza, G.L. (2008). Tumor metabolism: cancer cells give and take lactate. The Journal of clinical investigation *118*, 3835-3837.

Semenza, G.L. (2012). Hypoxia-inducible factors in physiology and medicine. Cell *148*, 399-408.

Shimozaki, K., Clemenson, G.D., Jr., and Gage, F.H. (2013). Paired related homeobox protein 1 is a regulator of stemness in adult neural stem/progenitor cells. J Neurosci *33*, 4066-4075.

Smetana, H.F., and Scott, W.F., Jr. (1951). Malignant tumors of nonchromaffin paraganglia. Mil Surg *109*, 330-349.

Sonveaux, P., Vegran, F., Schroeder, T., Wergin, M.C., Verrax, J., Rabbani, Z.N., De Saedeleer, C.J., Kennedy, K.M., Diepart, C., Jordan, B.F., *et al.* (2008). Targeting lactate-fueled respiration selectively kills hypoxic tumor cells in mice. The Journal of clinical investigation *118*, 3930-3942.

Soriano, P. (1999). Generalized lacZ expression with the ROSA26 Cre reporter strain. Nat Genet *21*, 70-71.

UU IR Author Manuscript

Stanley, W.C. (1991). Myocardial lactate metabolism during exercise. Med Sci Sports Exerc *23*, 920-924.

Stockwin, L.H., Vistica, D.T., Kenney, S., Schrump, D.S., Butcher, D.O., Raffeld, M., and Shoemaker, R.H. (2009). Gene expression profiling of alveolar soft-part sarcoma (ASPS). BMC cancer *9*, 22.

Straessler, K.M., Jones, K.B., Hu, H., Jin, H., van de Rijn, M., and Capecchi, M.R. (2013). Modeling clear cell sarcomagenesis in the mouse: cell of origin differentiation state impacts tumor characteristics. Cancer Cell *23*, 215-227.

Subramanian, A., Tamayo, P., Mootha, V.K., Mukherjee, S., Ebert, B.L., Gillette, M.A., Paulovich, A., Pomeroy, S.L., Golub, T.R., Lander, E.S.*, et al.* (2005). Gene set enrichment analysis: a knowledge-based approach for interpreting genome-wide expression profiles. Proc Natl Acad Sci U S A *102*, 15545-15550.

Vistica, D.T., Hollingshead, M., Borgel, S.D., Kenney, S., Stockwin, L.H., Raffeld, M., Schrump, D.S., Burkett, S., Stone, G., Butcher, D.O.*, et al.* (2009). Therapeutic vulnerability of an in vivo model of alveolar soft part sarcoma (ASPS) to antiangiogenic therapy. Journal of pediatric hematology/oncology *31*, 561-570.

Walenta, S., Salameh, A., Lyng, H., Evensen, J.F., Mitze, M., Rofstad, E.K., and Mueller-Klieser, W. (1997). Correlation of high lactate levels in head and neck tumors with incidence of metastasis. Am J Pathol *150*, 409-415.

UU IR Author Manuscript

Walenta, S., Schroeder, T., and Mueller-Klieser, W. (2004). Lactate in solid malignant tumors: potential basis of a metabolic classification in clinical oncology. Curr Med Chem *11*, 2195-2204.

Xiong, M., Elson, G., Legarda, D., and Leibovich, S.J. (1998). Production of vascular endothelial growth factor by murine macrophages: regulation by hypoxia, lactate, and the inducible nitric oxide synthase pathway. Am J Pathol *153*, 587-598.

Zambon, A.C., Gaj, S., Ho, I., Hanspers, K., Vranizan, K., Evelo, C.T., Conklin, B.R., Pico, A.R., and Salomonis, N. (2012). GO-Elite: a flexible solution for pathway and ontology over-representation. Bioinformatics *28*, 2209-2210.

UU IR Author Manuscript

Figure Legends

Figure 1. A mouse allele with conditional expression of human *ASPSCR1-TFE3*.

(A) Schematic demonstrating generation of the fusion transcript in human alveolar soft part sarcoma, which was reverse transcribed to a complementary DNA (cDNA) and targeted to the Rosa26 locus, separated from its promoter by a loxP-flanked stop sequence consisting of the neomycin resistance gene (neoR) and a poly-adenylation transcription termination sequence. The cDNA is followed by enhanced green fluorescent protein (eGFP) and internal ribosomal entry site (IRES), such that both the fusion gene and eGFP will be translated from the same transcript following Cre-mediated recombination to remove the stop. (B) Photomicrographs of embryonic day 12.5 *Rosa26*$^{LSL\text{-}AT3}/_{wt}$ fibroblasts 48 hours after exposure to TATCre or control, demonstrating GFP fluorescence from the recombined allele and (C) reverse transcriptase polymerase chain reaction (RT-PCR) showing presence of the fusion gene transcript following TATCre, but not control.

Figure 2. *ASPSCR1-TFE3* induces rapid tumorigenesis, restricted to the cranium.
(A) Chart depicting the relative rates of tumorigenesis and (B) diagrams of the anatomic distribution of tumors among *Rosa26*-$^{LSL\text{-}EWSR1\text{-}ATF1}/_{CreER}$, *Rosa26*-$^{LSL\text{-}SS18\text{-}SSX2}/_{CreER}$, and *Rosa26*-$^{LSL\text{-}AT3}/_{CreER}$ mice. Lateral cranium radiographs (C-D), gross dissection mid-sagittal brain photos (E-F), and GFP fluorescence photos (G-H) of 3 month old *Rosa26*-$^{LSL\text{-}AT3}/_{CreER}$ (C, E, G) and *Rosa26*-$^{LSL\text{-}AT3}/_{wt}$ (D, F, H) mice showing occipital expansion (between black arrows, C) from a tumor that developed in the brain (white arrows, E

and G) and demonstrates GFP fluorescence from the active *AT3* allele. Representative photomicrographs of the gamut of intra-cranial tumor presentations in *Rosa26-*$^{LSL\text{-}AT3}/_{CreER}$ mice, in which most were intra-parenchymal (I), but one encroached on the choroid plexus (J) and another developed within the eye (K).

Figure 3. *ASPSCR1-TFE3*-induced mouse tumors recapitulate human alveolar soft part sarcoma diagnostic histopathology.

(A) Low- and (B) high-power hematoxylin and eosin photomicrographs from tumors arising in *Rosa26-*$^{LSL\text{-}AT3}/_{CreER}$ mice match those from human ASPSs (C and D) in the overall tissue architecture of loosely nesting cells between arcading capillary networks and cellular features of round large nuclei with prominent nucleoli. (E) Photomicrograph of diastase-resistant periodic acid Schiff staining identifies the pathognomonic cytoplasmic granules (black arrows) in *Rosa26-*$^{LSL\text{-}AT3}/_{CreER}$ mouse tumors and human ASPSs (F). Clinical immunohistochemistry against human TFE3 demonstrates strong nuclear staining in both *Rosa26-*$^{LSL\text{-}AT3}/_{CreER}$ mouse tumors (G) and human ASPSs (H). H&E photomicrographs demonstrate a tumor growing between sulci near the investing pia mater (arrows in I), which was sometimes maintained between the tumor cells and the surrounding tissues (arrows in J); other invading tumor cells into the cerebellum (K), cerebral cortex (L), and choroid plexus (M) maintained no intervening leptomeningeal layer, but often associated closely with small vessels (arrows in N). (All scale bars and the width of panels B, D, E, and F are 40μm in length.)

UU IR Author Manuscript

Figure 4. *ASPSCR1-TFE3*-induced mouse tumors recapitulate human alveolar soft part sarcoma by transcriptome profile.

(A) Series of Broad Institute gene set enrichment analysis (GSEA) plots testing the 500 most significantly up-regulated (left, in each pair) and down-regulated (right, in each pair) genes from the *Rosa26-*$^{LSL\text{-}AT3}$*/*$_{CreER}$ mouse tumor (mASPS) to muscle RNAseq comparison, the human alveolar soft part sarcoma (hASPS) to muscle RNAseq comparison, and the human ASPS to muscle microarray comparison (GEO), in each of the other data sets. All of the up-regulated gene lists had high normalized enrichment scores (NES) and were statistically significant with false discover rate q-values less than 0.0005. None of the down-regulated gene lists showed enrichment. (B) Heat map of log2 transformed fold-changes from the control mean of the 539 genes with at least 2-fold and significant mean up-regulation in all three data sets. (C) Chart of the Z-scores of the most significant biological process gene ontologies from GO-Elite analysis of the 539 genes up-regulated in all three data sets.

Figure 5. *ASPSCR1-TFE3*-induced tumorigenesis is most efficient within the cranium.

(A) Diagram depicting the relative incidence and representative histopathology of the two grouped anatomic locations of tumors arising *Prx1-CreERT2;Rosa26-*$^{LSL\text{-}AT3}$*/*$_{wt}$ mice after receiving tamoxifen at age 2 weeks, intra-cranial periosteum and in the brain parenchyma, but not in the extra-cranial periosteum or the limb. (B) Photomicrographs of X-gal-stained sections from the cranium's inner and outer tables, as well as the

proximal humerus in 3 week old *Prx1-CreERT2;Rosa26-*$^{LacZ}/_{wt}$ mice after receiving tamoxifen at age 2 weeks, demonstrating the *Prx1-CreERT2* lineage in each location (blue cells identified by black arrows), only the first of which led to identifiable tumorigenesis when initiating the *AT3* allele. (Scale bars in A and panel widths in B are each 100μm in length.)

Figure 6. *ASPSCR1-TFE3*-induced mouse tumor lactate transport gene expression and tissue lactate levels in the mouse.

(A) Chart of the gene expression by fragments per kilobase of exon per million fragments mapped (FPKM) in *Rosa26-*$^{LSL\text{-}AT3}/_{CreER}$ mouse tumors (red) and muscle samples (black), showing high and significantly up-regulated expression of both *Cd147* and *Mct1* in tumors and low and significantly down-regulated expression of *Mct4*. (B) Plot of the individual (dots) and mean (bars) concentrations of lactate in the tissues of 5 mice, determined biochemically.

Figure 7. *ASPSCR1-TFE3*-induced mouse tumors and human alveolar soft part sarcomas can metabolize lactate.

Heat maps from *Rosa26-*$^{LSL\text{-}AT3}/_{CreER}$ mouse tumors (A) and human alveolar soft part sarcomas (B) showing the log2 ratios of expression normalized to the mean for the Broad Institute's curated MitoCarta gene list. (C) Chart of the mean ± standard deviation of the oxygen consumption rate (normalized by DNA content) of tissue sections from tumors arising in mice induced by each of three fusion oncogenes, representing alveolar soft part sarcoma, synovial sarcoma, and clear cell sarcoma (n = 10 for each). (D) Chart

UU IR Author Manuscript

of the mean ± standard deviation of the percent change in oxygen consumption among fresh tissue section from three mouse tumor types upon administration of 10mM lactate substrate (n = 5 for each).

Figure 8. *ASPSCR1-TFE3*-induced mouse tumors express hypoxia genes in the absence of hypoxia and respond to exogenous lactate.

(A) Explanatory diagram of the pathway by which either hypoxia or imported lactate can decrease 2-oxoglutarate-mediated Hif1α hydroxylation and degradation (Lu et al., 2002) (Lu et al., 2005). (B) Photomicrographs of pimonidazole-treated *Rosa26-*$^{LSL\text{-}AT3}/_{CreER}$ mouse tumor and kidney tissue sections stained with immunohistochemistry against pimonidazole adducts (above; brown depicts presence of hypoxia) and Hif1α (below), demonstrating nuclear Hif1α, but no hypoxia in tumors, and Hif1α correlating to hypoxia in normal renal tubules. (C) Broad Institute gene set enrichment analysis for the established Harris hypoxia gene list in the *Rosa26-*$^{LSL\text{-}AT3}/_{CreER}$ mouse tumor (mASPS) to muscle RNAseq comparison, showing upregulation of many ostensibly hypoxia-driven genes in the tumors. (Scale bars are 10μm in length.) (D) Representative photomicrographs of immunohistochemistry against Ki-67, indicating proliferating nuclei (brown) or Cd31, indicating vascular endothelial cells (brown) after 2 weeks of lactate or saline administration to *Rosa26-*$^{LSL\text{-}AT3}/_{CreER}$ mice bearing tumors. (E) Chart of the mean ± standard deviation of the ratio of Ki-67-positive tumor cell nuclei to total tumor cell nuclei between the two groups (n = 5 lactate and 7 saline controls). (F) Chart of the mean ± standard deviation of the ratio of the linear vessel perimeter to total tumor cell nuclei between the two groups (n = 5 lactate and 7 saline controls). (G) Charts

UU IR Author Manuscript

presenting mean ± standard deviation of the relative viability of ASPSCR1-TFE3-expressing human cancer cell lines FU-UR-1 (at 48 hours) and ASPS-1 (at 72 hours) in increasing concentrations of sodium lactate (n = 3 for each point; experiments also repeated). (I) Western blots showing increased nuclear HIF1α when exposed to 20mM sodium lactate that is blocked by the MCT1-inhibitor, CHC at 0.1mM in FU-UR-1 cells and 1mM in ASPS-1 cells.

UU IR Author Manuscript

Figure 1
Click here to download high resolution image

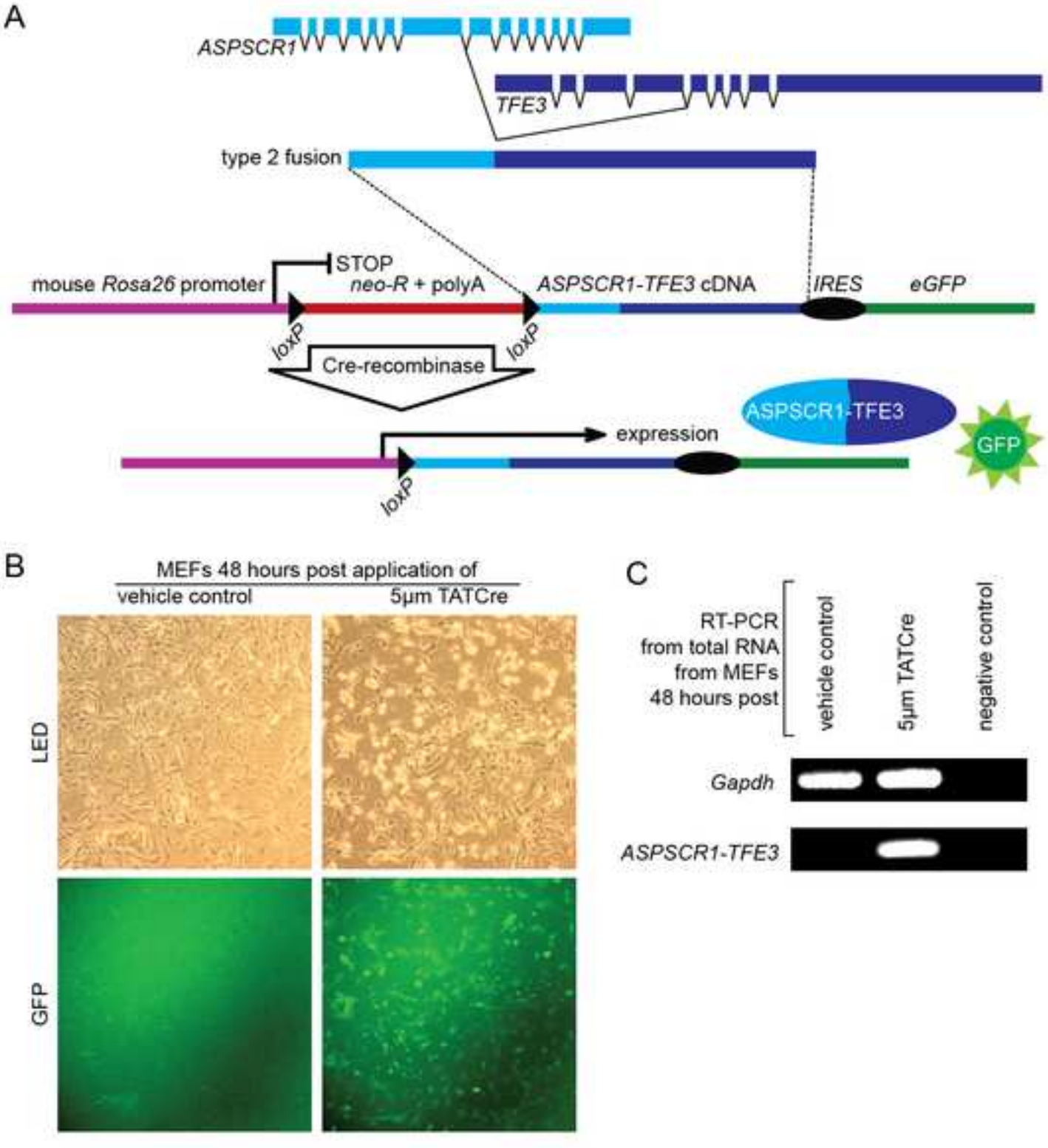

Figure 2
Click here to download high resolution image

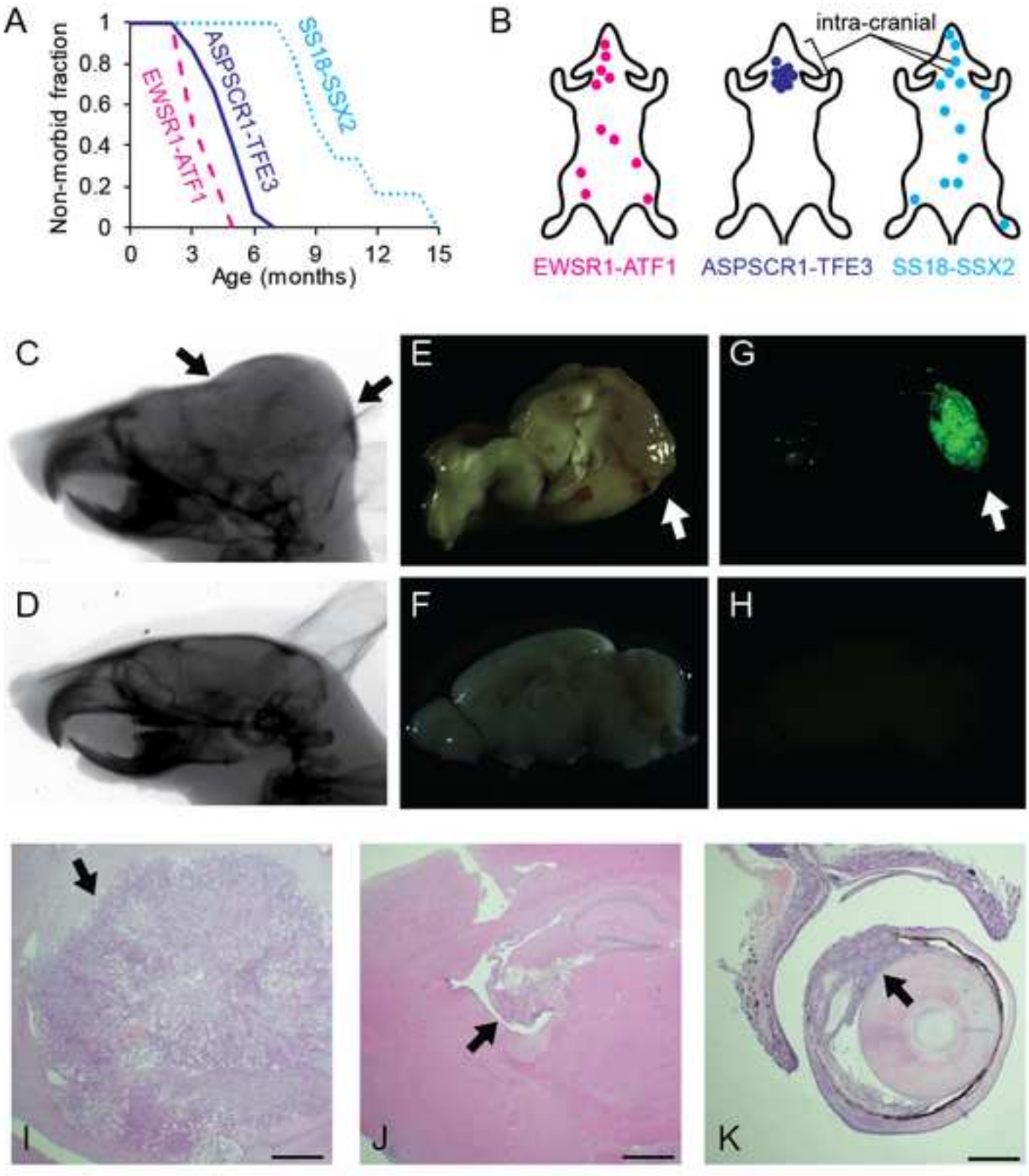

Figure 3 (revised again)
Click here to download high resolution image

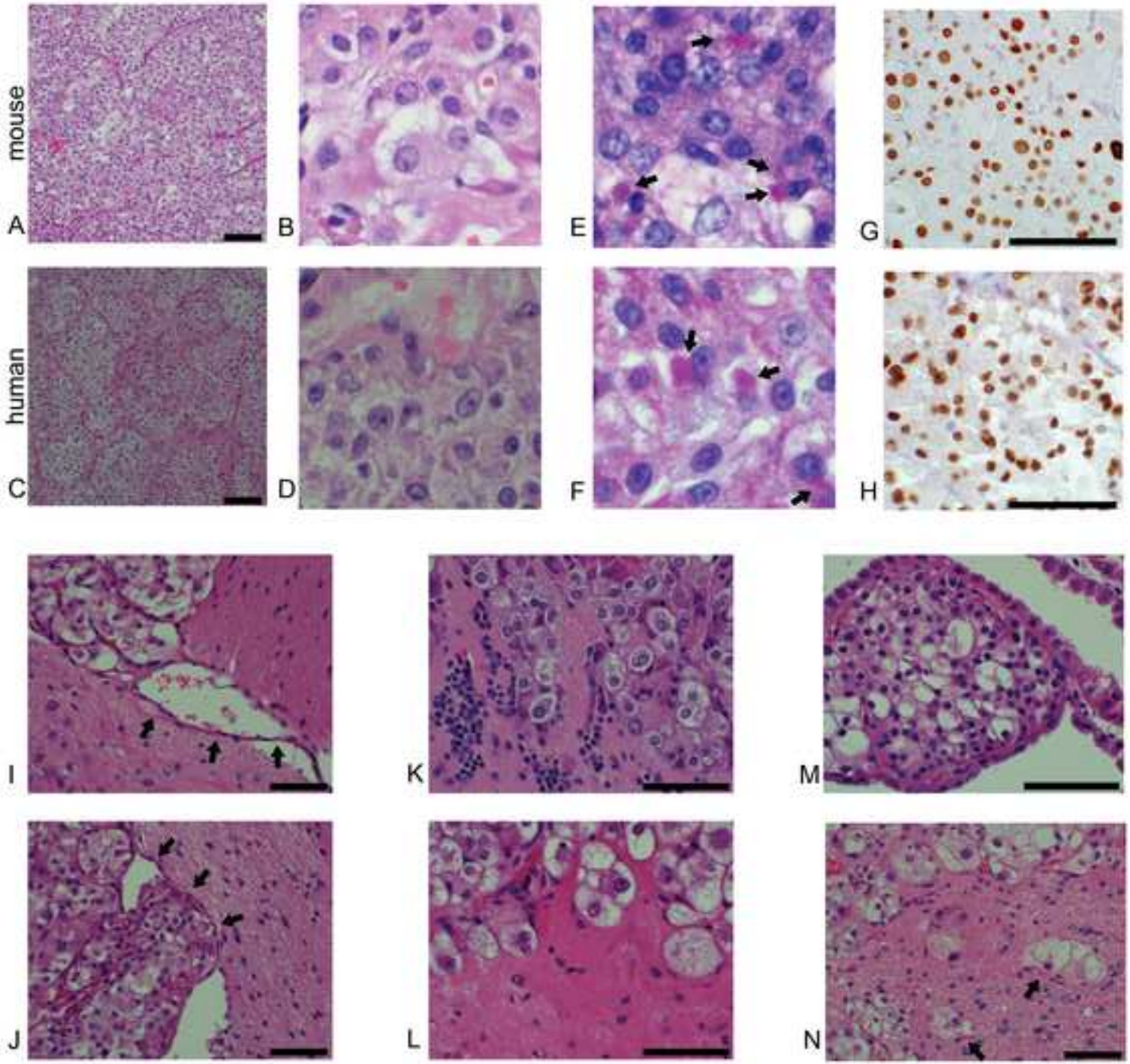

Figure 4
Click here to download high resolution image

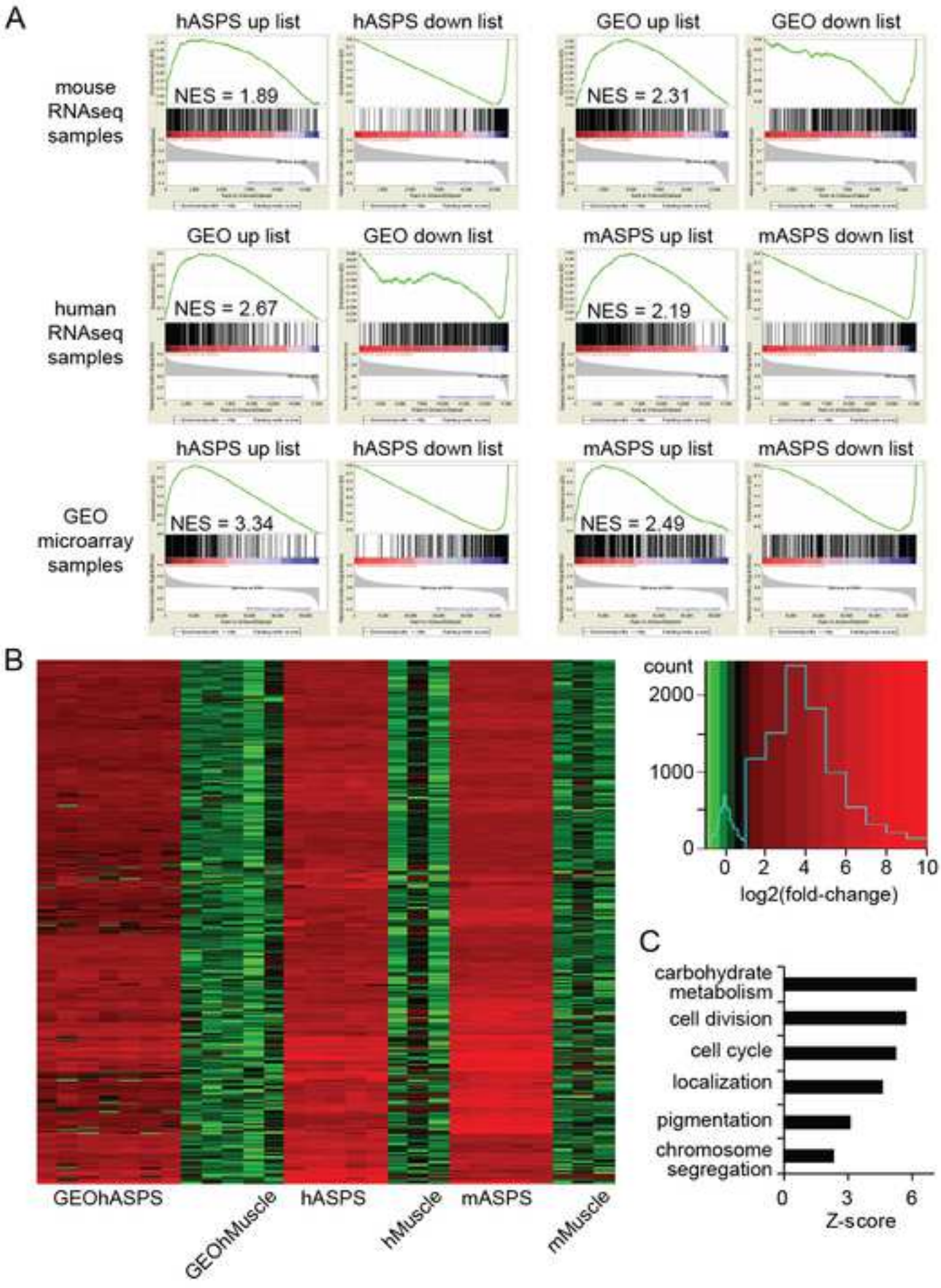

Figure 5 (revised)
Click here to download high resolution image

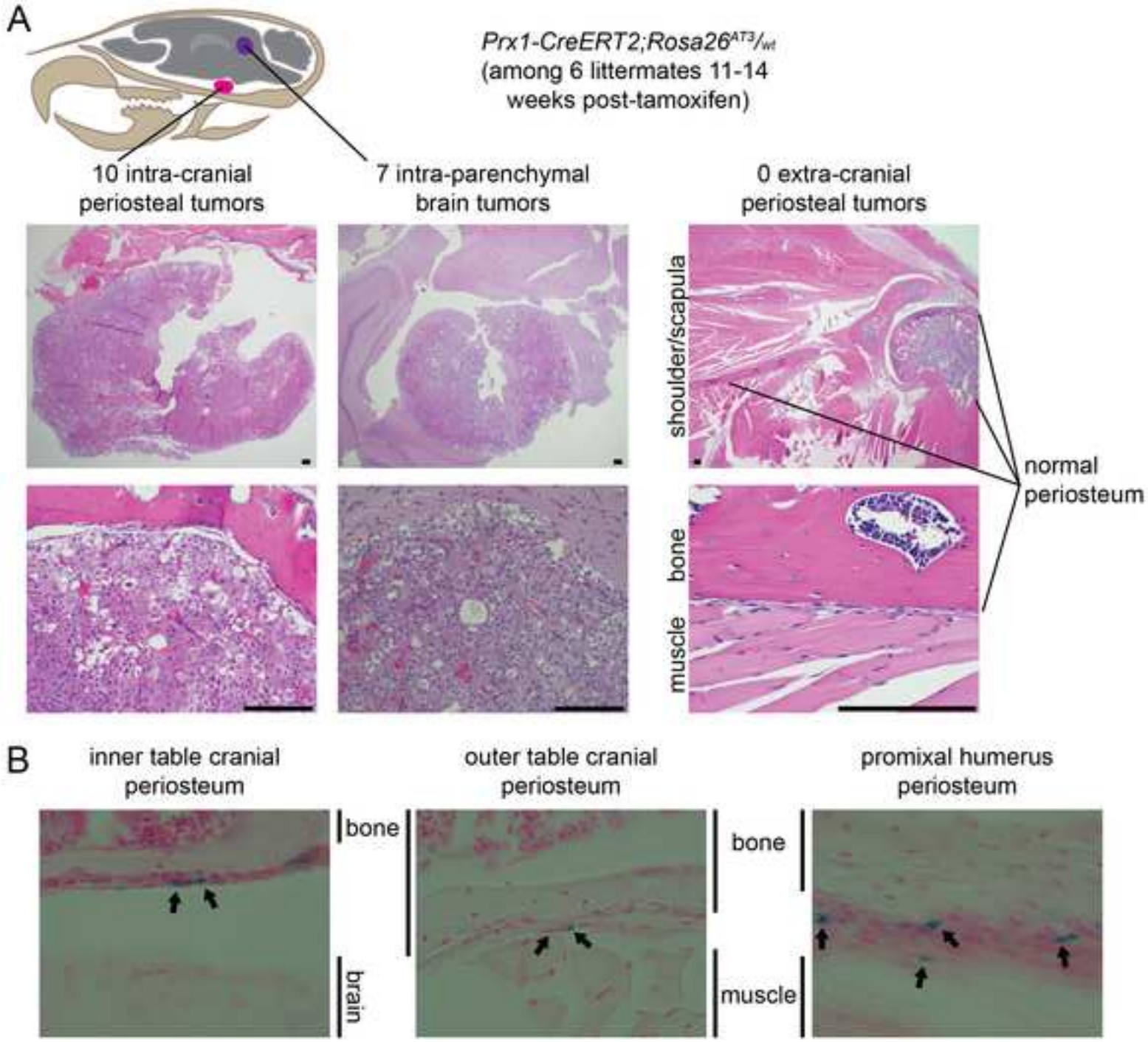

Figure 6 (revised)
Click here to download high resolution image

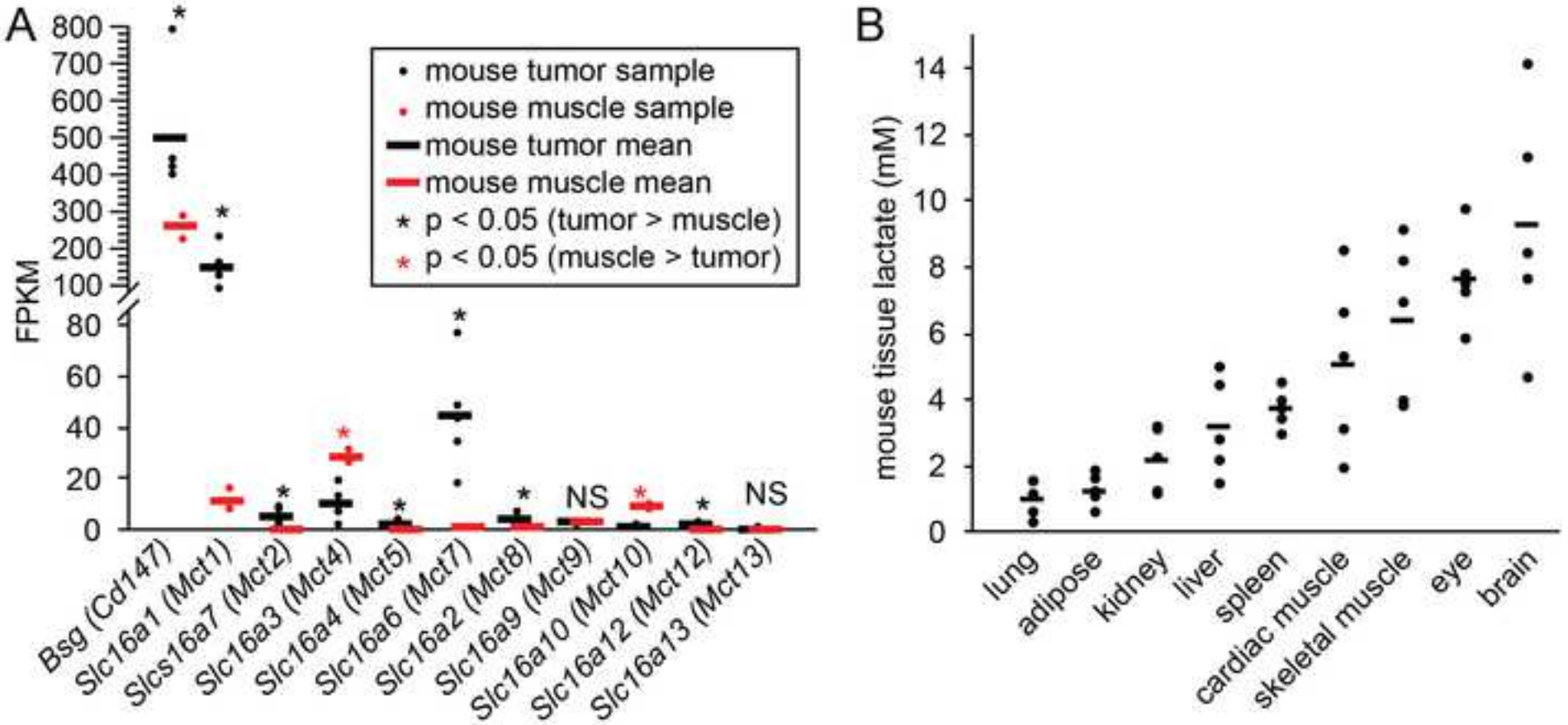

Figure 7 (revised)
Click here to download high resolution image

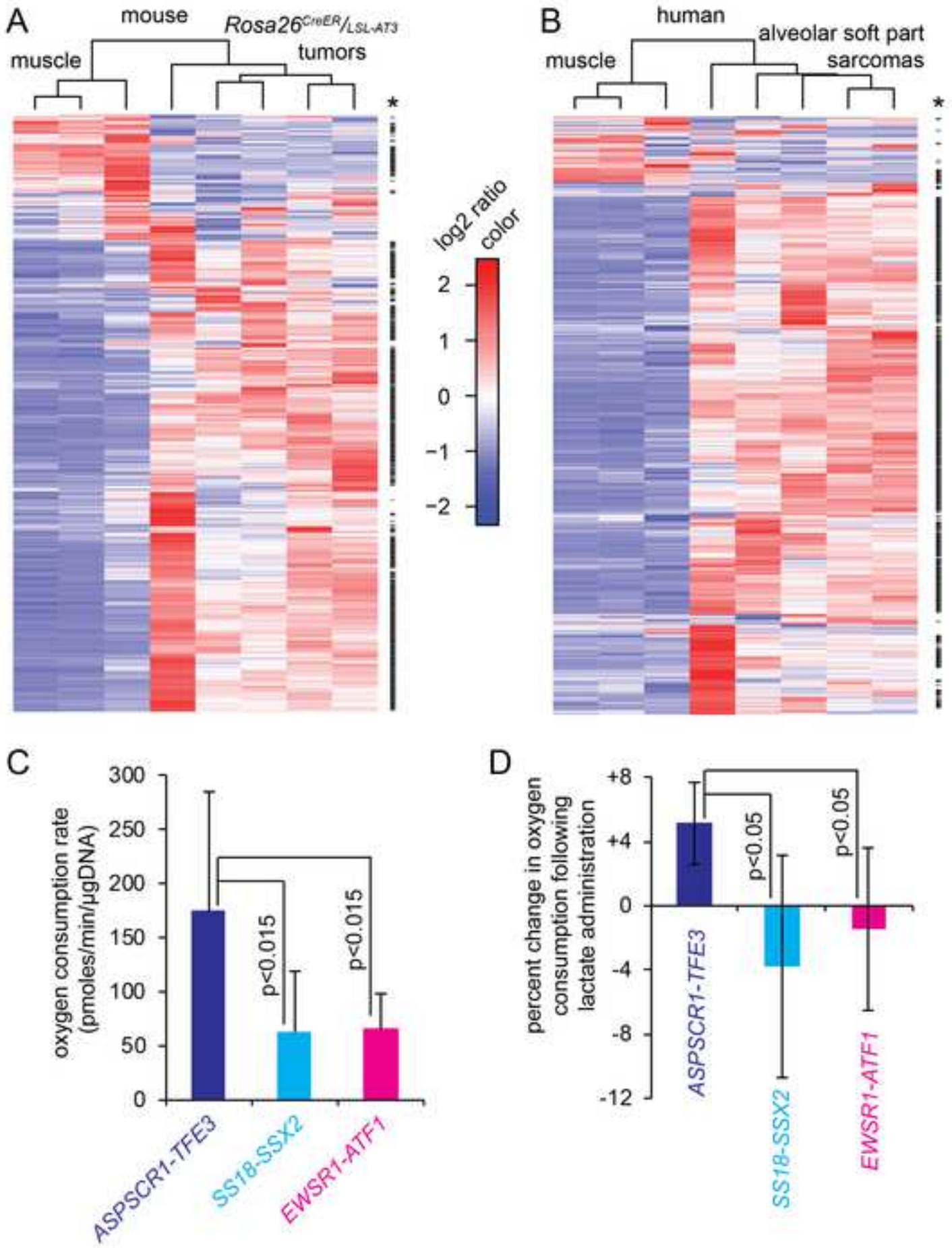

Figure 8 (revised again)
Click here to download high resolution image

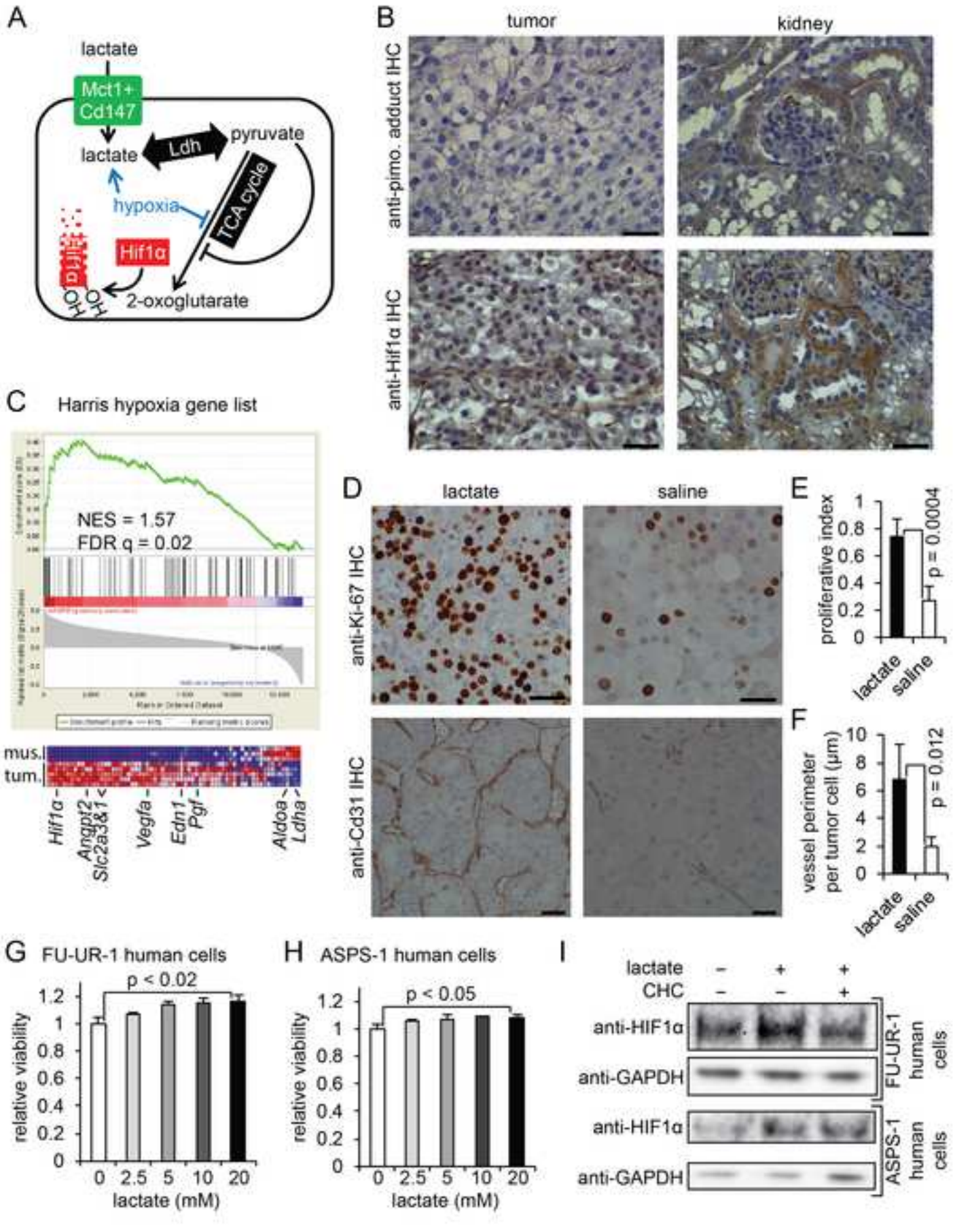

Inventory of Supplemental Information:

Supplemental Table 1
Supplemental Experimental Procedures

Supplemental Text & Figures
Click here to download Supplemental Text & Figures: SupplementalInformation.pdf

Supplemental Table 1. Genes 2-fold and significantly up-regulated in mouse and both human data sets comparing *ASPSCR1-TFE3*-driven tumors to skeletal muscle controls.

Human ENSEMBL#	Probe on HU133+2.0	Human Gene Symbol	Mouse Gene Symbol
ENSG00000001036	223120_at	*FUCA2*	*Fuca2*
ENSG00000002933	218345_at	*TMEM176A*	*Tmem176a*
ENSG00000004864	229061_s_at	*SLC25A13*	*Slc25a13*
ENSG00000005022	200657_at	*SLC25A5*	*Slc25a5*
ENSG00000005893	203041_s_at	*LAMP2*	*Lamp2*
ENSG00000006075	205114_s_at	*CCL3*	*Ccl3*
ENSG00000006118	218834_s_at	*TMEM132A*	*Tmem132a*
ENSG00000006634	204244_s_at	*DBF4*	*Dbf4*
ENSG00000007372	235795_at	*PAX6*	*Pax6*
ENSG00000008394	1565162_s_at	*MGST1*	*Mgst1*
ENSG00000011304	212016_s_at	*PTBP1*	*Ptbp1*
ENSG00000011426	1552619_a_at	*ANLN*	*Anln*
ENSG00000012124	38521_at	*CD22*	*Cd22*
ENSG00000013288	214703_s_at	*MAN2B2*	*Man2b2*
ENSG00000013306	223649_s_at	*SLC25A39*	*Slc25a39*
ENSG00000019505	226086_at	*SYT13*	*Syt13*
ENSG00000019549	213139_at	*SNAI2*	*Snai2*
ENSG00000023171	212906_at	*GRAMD1B*	*Gramd1b*
ENSG00000024526	222958_s_at	*DEPDC1*	*Depdc1a*
ENSG00000030582	211284_s_at	*GRN*	*Grn*
ENSG00000035499	226980_at	*DEPDC1B*	*Depdc1b*
ENSG00000035862	203167_at	*TIMP2*	*Timp2*
ENSG00000039560	202052_s_at	*RAI14*	*Rai14*
ENSG00000041515	1557720_s_at	*MYO16*	*Myo16*
ENSG00000043462	205269_at	*LCP2*	*Lcp2*
ENSG00000049860	201944_at	*HEXB*	*Hexb*
ENSG00000050165	214247_s_at	*DKK3*	*Dkk3*
ENSG00000052795	225924_at	*FNIP2*	*Fnip2*
ENSG00000054690	225726_s_at	*PLEKHH1*	*Plekhh1*
ENSG00000055732	220484_at	*MCOLN3*	*Mcoln3*
ENSG00000057019	224911_s_at	*DCBLD2*	*Dcbld2*
ENSG00000057252	228479_at	*SOAT1*	*Soat1*
ENSG00000059573	222416_at	*ALDH18A1*	*Aldh18a1*
ENSG00000060709	214811_at	*RIMBP2*	*Rimbp2*
ENSG00000060982	226517_at	*BCAT1*	*Bcat1*
ENSG00000064666	201605_x_at	*CNN2*	*Cnn2*
ENSG00000066279	219918_s_at	*ASPM*	*Aspm*
ENSG00000066322	218028_at	*ELOVL1*	*Elovl1*
ENSG00000066468	208229_at	*FGFR2*	*Fgfr2*
ENSG00000067057	201037_at	*PFKP*	*Pfkp*
ENSG00000067167	201398_s_at	*TRAM1*	*Tram1*

Human ENSEMBL#	Probe on HU133+2.0	Human Gene Symbol	Mouse Gene Symbol
ENSG00000069424	203402_at	*KCNAB2*	*Kcnab2*
ENSG00000069849	208836_at	*ATP1B3*	*Atp1b3*
ENSG00000069966	204000_at	*GNB5*	*Gnb5*
ENSG00000069974	209515_s_at	*RAB27A*	*Rab27a*
ENSG00000070669	205047_s_at	*ASNS*	*Asns*
ENSG00000072041	232263_at	*SLC6A15*	*Slc6a15*
ENSG00000072110	208637_x_at	*ACTN1*	*Actn1*
ENSG00000072571	207165_at	*HMMR*	*Hmmr*
ENSG00000074696	222404_x_at	*PTPLAD1*	*Ptplad1*
ENSG00000074800	201231_s_at	*ENO1*	*Eno1*
ENSG00000075618	210933_s_at	*FSCN1*	*Fscn1*
ENSG00000075624	AFFX-HSAC07/X00351_M_at	*ACTB*	*Actb*
ENSG00000076944	209367_at	*STXBP2*	*Stxbp2*
ENSG00000077585	204137_at	*GPR137B*	*Gpr137b*
ENSG00000080824	211969_at	*HSP90AA1*	*Hsp90aa1*
ENSG00000080986	204162_at	*NDC80*	*Ndc80*
ENSG00000081087	218196_at	*OSTM1*	*Ostm1*
ENSG00000081803	219572_at	*CADPS2*	*Cadps2*
ENSG00000083720	202780_at	*OXCT1*	*Oxct1*
ENSG00000083857	201579_at	*FAT1*	*Fat1*
ENSG00000085733	201059_at	*CTTN*	*Cttn*
ENSG00000087077	209129_at	*TRIP6*	*Trip6*
ENSG00000087088	211833_s_at	*BAX*	*Bax*
ENSG00000087253	239598_s_at	*LPCAT2*	*Lpcat2*
ENSG00000087448	225732_at	*KLHDC5*	*Klhl42*
ENSG00000088367	212336_at	*EPB41L1*	*Epb4.1l1*
ENSG00000090889	218355_at	*KIF4A*	*Kif4*
ENSG00000091129	204105_s_at	*NRCAM*	*Nrcam*
ENSG00000091428	205651_x_at	*RAPGEF4*	*Rapgef4*
ENSG00000091651	219105_x_at	*ORC6*	*Orc6*
ENSG00000091879	237261_at	*ANGPT2*	*Angpt2*
ENSG00000092445	211431_s_at	*TYRO3*	*Tyro3*
ENSG00000092820	208623_s_at	*EZR*	*Ezr*
ENSG00000092853	243840_at	*CLSPN*	*Clspn*
ENSG00000094804	203968_s_at	*CDC6*	*Cdc6*
ENSG00000095383	222173_s_at	*TBC1D2*	*Tbc1d2*
ENSG00000095397	221887_s_at	*DFNB31*	*Whrn*
ENSG00000097046	204510_at	*CDC7*	*Cdc7*
ENSG00000099194	223839_s_at	*SCD*	*Scd2*
ENSG00000099377	222817_at	*HSD3B7*	*Hsd3b7*
ENSG00000100075	210010_s_at	*SLC25A1*	*Slc25a1*
ENSG00000100167	223362_s_at	*41520*	*3-Sep*
ENSG00000100292	203665_at	*HMOX1*	*Hmox1*
ENSG00000100297	201755_at	*MCM5*	*Mcm5*
ENSG00000100299	204443_at	*ARSA*	*Arsa*
ENSG00000100526	1555758_a_at	*CDKN3*	*Cdkn3*

Human ENSEMBL#	Probe on HU133+2.0	Human Gene Symbol	Mouse Gene Symbol
ENSG00000100644	200989_at	*HIF1A*	*Hif1a*
ENSG00000100889	202847_at	*PCK2*	*Pck2*
ENSG00000100979	202075_s_at	*PLTP*	*Pltp*
ENSG00000100994	201481_s_at	*PYGB*	*Pygb*
ENSG00000100997	224742_at	*ABHD12*	*Abhd12*
ENSG00000101160	210042_s_at	*CTSZ*	*Ctsz*
ENSG00000101224	201853_s_at	*CDC25B*	*Cdc25b*
ENSG00000101255	218145_at	*TRIB3*	*Trib3*
ENSG00000101349	210721_s_at	*PAK7*	*Pak7*
ENSG00000101350	225205_at	*KIF3B*	*Kif3b*
ENSG00000101412	2028_s_at	*E2F1*	*E2f1*
ENSG00000101577	202459_s_at	*LPIN2*	*Lpin2*
ENSG00000101680	227048_at	*LAMA1*	*Lama1*
ENSG00000101773	203344_s_at	*RBBP8*	*Rbbp8*
ENSG00000101850	206696_at	*GPR143*	*Gpr143*
ENSG00000101856	201121_s_at	*PGRMC1*	*Pgrmc1*
ENSG00000101911	230352_at	*PRPS2*	*Prps2*
ENSG00000102032	206617_s_at	*RENBP*	*Renbp*
ENSG00000102096	204269_at	*PIM2*	*Pim2*
ENSG00000102221	204866_at	*PHF16*	*Phf16*
ENSG00000102265	201666_at	*TIMP1*	*Timp1*
ENSG00000102393	214430_at	*GLA*	*Gla*
ENSG00000103034	209159_s_at	*NDRG4*	*Ndrg4*
ENSG00000103249	38069_at	*CLCN7*	*Clcn7*
ENSG00000103257	201195_s_at	*SLC7A5*	*Slc7a5*
ENSG00000103855	224859_at	*CD276*	*Cd276*
ENSG00000103888	212942_s_at	*KIAA1199*	*9930013L23Rik*
ENSG00000104093	212820_at	*DMXL2*	*Dmxl2*
ENSG00000104361	220128_s_at	*NIPAL2*	*Nipal2*
ENSG00000104490	211685_s_at	*NCALD*	*Ncald*
ENSG00000104549	209218_at	*SQLE*	*Sqle*
ENSG00000104723	209228_x_at	*TUSC3*	*Tusc3*
ENSG00000105011	218115_at	*ASF1B*	*Asf1b*
ENSG00000105223	201050_at	*PLD3*	*Pld3*
ENSG00000105402	206491_s_at	*NAPA*	*Napa*
ENSG00000105486	202726_at	*LIG1*	*Lig1*
ENSG00000105699	208190_s_at	*LSR*	*Lsr*
ENSG00000105939	225634_at	*ZC3HAV1*	*Zc3hav1*
ENSG00000106266	228231_at	*SNX8*	*Snx8*
ENSG00000106565	220532_s_at	*TMEM176B*	*Tmem176b*
ENSG00000106617	222582_at	*PRKAG2*	*Prkag2*
ENSG00000106624	201792_at	*AEBP1*	*Aebp1*
ENSG00000106772	212805_at	*PRUNE2*	*Prune2*
ENSG00000107249	230258_at	*GLIS3*	*Glis3*
ENSG00000107521	217354_s_at	*HPS1*	*Hps1*
ENSG00000107731	226899_at	*UNC5B*	*Unc5b*

Human ENSEMBL#	Probe on HU133+2.0	Human Gene Symbol	Mouse Gene Symbol
ENSG00000108375	218704_at	*RNF43*	*Rnf43*
ENSG00000108784	204360_s_at	*NAGLU*	*Naglu*
ENSG00000108828	208626_s_at	*VAT1*	*Vat1*
ENSG00000109062	201349_at	*SLC9A3R1*	*Slc9a3r1*
ENSG00000109103	203271_s_at	*UNC119*	*Unc119*
ENSG00000109265	227230_s_at	*KIAA1211*	*C530008M17Rik*
ENSG00000109323	203778_at	*MANBA*	*Manba*
ENSG00000109436	212960_at	*TBC1D9*	*Tbc1d9*
ENSG00000109654	202341_s_at	*TRIM2*	*Trim2*
ENSG00000109805	218662_s_at	*NCAPG*	*Ncapg*
ENSG00000109819	219195_at	*PPARGC1A*	*Ppargc1a*
ENSG00000109854	209448_at	*HTATIP2*	*Htatip2*
ENSG00000110090	203633_at	*CPT1A*	*Cpt1a*
ENSG00000110092	208711_s_at	*CCND1*	*Ccnd1*
ENSG00000110492	209035_at	*MDK*	*Mdk*
ENSG00000110880	221676_s_at	*CORO1C*	*Coro1c*
ENSG00000111110	212686_at	*PPM1H*	*Ppm1h*
ENSG00000111206	202580_x_at	*FOXM1*	*Foxm1*
ENSG00000111229	208736_at	*ARPC3*	*Arpc3*
ENSG00000111412	222767_s_at	*C12orf49*	*2410131K14Rik*
ENSG00000111432	219764_at	*FZD10*	*Fzd10*
ENSG00000111602	203046_s_at	*TIMELESS*	*Timeless*
ENSG00000111670	240106_at	*GNPTAB*	*Gnptab*
ENSG00000111674	201313_at	*ENO2*	*Eno2*
ENSG00000111816	207178_s_at	*FRK*	*Frk*
ENSG00000112379	231856_at	*KIAA1244*	*D10Bwg1379e*
ENSG00000112742	204822_at	*TTK*	*Ttk*
ENSG00000112799	205859_at	*LY86*	*Ly86*
ENSG00000112977	201095_at	*DAP*	*Dap*
ENSG00000112984	218755_at	*KIF20A*	*Kif20a*
ENSG00000113361	205532_s_at	*CDH6*	*Cdh6*
ENSG00000113552	202382_s_at	*GNPDA1*	*Gnpda1*
ENSG00000113732	200096_s_at	*ATP6V0E1*	*Atp6v0e*
ENSG00000113805	229831_at	*CNTN3*	*Cntn3*
ENSG00000113810	201663_s_at	*SMC4*	*Smc4*
ENSG00000114346	234992_x_at	*ECT2*	*Ect2*
ENSG00000114573	201972_at	*ATP6V1A*	*Atp6v1a*
ENSG00000114757	241833_at	*PEX5L*	*Pex5l*
ENSG00000115738	201565_s_at	*ID2*	*Id2*
ENSG00000115884	201287_s_at	*SDC1*	*Sdc1*
ENSG00000116675	204720_s_at	*DNAJC6*	*Dnajc6*
ENSG00000116954	218088_s_at	*RRAGC*	*Rragc*
ENSG00000116991	233587_s_at	*SIPA1L2*	*Sipa1l2*
ENSG00000117322	205544_s_at	*CR2*	*Cr2*
ENSG00000117394	201250_s_at	*SLC2A1*	*Slc2a1*
ENSG00000117410	200078_s_at	*ATP6V0B*	*Atp6v0b*

Human ENSEMBL#	Probe on HU133+2.0	Human Gene Symbol	Mouse Gene Symbol
ENSG00000117519	201445_at	*CNN3*	*Cnn3*
ENSG00000117643	218918_at	*MAN1C1*	*Man1c1*
ENSG00000117724	209172_s_at	*CENPF*	*Cenpf*
ENSG00000117984	200766_at	*CTSD*	*Ctsd*
ENSG00000118160	215267_s_at	*SLC8A2*	*Slc8a2*
ENSG00000118193	236641_at	*KIF14*	*Kif14*
ENSG00000118242	219648_at	*MREG*	*Mreg*
ENSG00000118508	204214_s_at	*RAB32*	*Rab32*
ENSG00000118596	207057_at	*SLC16A7*	*Slc16a7*
ENSG00000118785	209875_s_at	*SPP1*	*Spp1*
ENSG00000118855	218109_s_at	*MFSD1*	*Mfsd1*
ENSG00000118946	205656_at	*PCDH17*	*Pcdh17*
ENSG00000119408	223158_s_at	*NEK6*	*Nek6*
ENSG00000119537	202419_at	*KDSR*	*Kdsr*
ENSG00000119655	200701_at	*NPC2*	*Npc2*
ENSG00000119943	228384_s_at	*PYROXD2*	*Pyroxd2*
ENSG00000119969	223556_at	*HELLS*	*Hells*
ENSG00000120256	225060_at	*LRP11*	*Lrp11*
ENSG00000120539	228468_at	*MASTL*	*Mastl*
ENSG00000120742	200971_s_at	*SERP1*	*Serp1*
ENSG00000120875	226034_at	*DUSP4*	*Dusp4*
ENSG00000121064	218217_at	*SCPEP1*	*Scpep1*
ENSG00000121068	40560_at	*TBX2*	*Tbx2*
ENSG00000121966	209201_x_at	*CXCR4*	*Cxcr4*
ENSG00000123095	221530_s_at	*BHLHE41*	*Bhlhe41*
ENSG00000123131	201923_at	*PRDX4*	*Prdx4*
ENSG00000123219	222848_at	*CENPK*	*Cenpk*
ENSG00000123416	212639_x_at	*TUBA1B*	*Tuba1b*
ENSG00000123453	207889_at	*SARDH*	*Sardh*
ENSG00000123500	217428_s_at	*COL10A1*	*Col10a1*
ENSG00000123572	232771_at	*NRK*	*Nrk*
ENSG00000123836	238450_at	*PFKFB2*	*Pfkfb2*
ENSG00000123975	204170_s_at	*CKS2*	*Cks2*
ENSG00000123989	202175_at	*CHPF*	*Chpf*
ENSG00000124126	224909_s_at	*PREX1*	*Prex1*
ENSG00000124191	228737_at	*TOX2*	*Tox2*
ENSG00000124357	218231_at	*NAGK*	*Nagk*
ENSG00000124766	201417_at	*SOX4*	*Sox4*
ENSG00000124785	218625_at	*NRN1*	*Nrn1*
ENSG00000125249	214487_s_at	*RAP2A*	*Rap2a*
ENSG00000125633	219774_at	*CCDC93*	*Ccdc93*
ENSG00000126217	239636_at	*MCF2L*	*Mcf2l*
ENSG00000126787	203764_at	*DLGAP5*	*Dlgap5*
ENSG00000128245	201020_at	*YWHAH*	*Ywhah*
ENSG00000128656	212624_s_at	*CHN1*	*Chn1*
ENSG00000128973	1567080_s_at	*CLN6*	*Cln6*

Human ENSEMBL#	Probe on HU133+2.0	Human Gene Symbol	Mouse Gene Symbol
ENSG00000129925	221882_s_at	*TMEM8A*	*Tmem8*
ENSG00000130066	210592_s_at	*SAT1*	*Sat1*
ENSG00000130202	225418_at	*PVRL2*	*Pvrl2*
ENSG00000130203	212884_x_at	*APOE*	*Apoe*
ENSG00000130402	200601_at	*ACTN4*	*Actn4*
ENSG00000130513	229868_s_at	*GDF15*	*Gdf15*
ENSG00000130540	219425_at	*SULT4A1*	*Sult4a1*
ENSG00000130813	218429_s_at	*C19orf66*	*A230050P20Rik*
ENSG00000130816	201697_s_at	*DNMT1*	*Dnmt1*
ENSG00000131171	201311_s_at	*SH3BGRL*	*Sh3bgrl*
ENSG00000131236	213798_s_at	*CAP1*	*Cap1*
ENSG00000131711	214577_at	*MAP1B*	*Map1b*
ENSG00000131747	201292_at	*TOP2A*	*Top2a*
ENSG00000131910	206410_at	*NR0B2*	*Nr0b2*
ENSG00000132646	201202_at	*PCNA*	*Pcna*
ENSG00000132718	209198_s_at	*SYT11*	*Syt11*
ENSG00000133639	200920_s_at	*BTG1*	*Btg1*
ENSG00000134287	200011_s_at	*ARF3*	*Arf3*
ENSG00000134504	226246_at	*KCTD1*	*Kctd1*
ENSG00000135119	221908_at	*RNFT2*	*Rnft2*
ENSG00000135124	204088_at	*P2RX4*	*P2rx4*
ENSG00000135127	228320_x_at	*CCDC64*	*Ccdc64*
ENSG00000135269	202720_at	*TES*	*Tes*
ENSG00000135362	1555486_a_at	*PRR5L*	*Prr5l*
ENSG00000135404	200663_at	*CD63*	*Cd63*
ENSG00000135446	202246_s_at	*CDK4*	*Cdk4*
ENSG00000135506	200714_x_at	*OS9*	*Os9*
ENSG00000135596	218376_s_at	*MICAL1*	*Mical1*
ENSG00000135677	212334_at	*GNS*	*Gns*
ENSG00000135905	219279_at	*DOCK10*	*Dock10*
ENSG00000136059	209950_s_at	*VILL*	*Vill*
ENSG00000136193	201462_at	*SCRN1*	*Scrn1*
ENSG00000136205	217853_at	*TNS3*	*Tns3*
ENSG00000136235	201141_at	*GPNMB*	*Gpnmb*
ENSG00000136492	221703_at	*BRIP1*	*Brip1*
ENSG00000136830	223019_at	*FAM129B*	*Fam129b*
ENSG00000136868	203971_at	*SLC31A1*	*Slc31a1*
ENSG00000137267	204141_at	*TUBB2A*	*Tubb2a*
ENSG00000137269	218816_at	*LRRC1*	*Lrrc1*
ENSG00000137285	214023_x_at	*TUBB2B*	*Tubb2b*
ENSG00000137462	204924_at	*TLR2*	*Tlr2*
ENSG00000137501	232914_s_at	*SYTL2*	*Sytl2*
ENSG00000137672	217287_s_at	*TRPC6*	*Trpc6*
ENSG00000137752	211366_x_at	*CASP1*	*Casp1*
ENSG00000137807	204709_s_at	*KIF23*	*Kif23*
ENSG00000137812	1552680_a_at	*CASC5*	*Casc5*

Human ENSEMBL#	Probe on HU133+2.0	Human Gene Symbol	Mouse Gene Symbol
ENSG00000138166	209457_at	*DUSP5*	*Dusp5*
ENSG00000138180	218542_at	*CEP55*	*Cep55*
ENSG00000138311	206448_at	*ZNF365*	*Zfp365*
ENSG00000138316	230167_at	*ADAMTS14*	*Adamts14*
ENSG00000138650	228635_at	*PCDH10*	*Pcdh10*
ENSG00000138670	1554999_at	*RASGEF1B*	*Rasgef1b*
ENSG00000138778	205046_at	*CENPE*	*Cenpe*
ENSG00000138821	209267_s_at	*SLC39A8*	*Slc39a8*
ENSG00000139146	223038_s_at	*FAM60A*	*Fam60a*
ENSG00000139354	238756_at	*GAS2L3*	*Gas2l3*
ENSG00000139370	225043_at	*SLC15A4*	*Slc15a4*
ENSG00000139410	228274_at	*SDSL*	*Sdsl*
ENSG00000139514	212295_s_at	*SLC7A1*	*Slc7a1*
ENSG00000139734	229097_at	*DIAPH3*	*Diap3*
ENSG00000140030	214467_at	*GPR65*	*Gpr65*
ENSG00000140525	213007_at	*FANCI*	*Fanci*
ENSG00000140526	63825_at	*ABHD2*	*Abhd2*
ENSG00000140853	226474_at	*NLRC5*	*Nlrc5*
ENSG00000140859	209661_at	*KIFC3*	*Kifc3*
ENSG00000140937	207172_s_at	*CDH11*	*Cdh11*
ENSG00000141012	206335_at	*GALNS*	*Galns*
ENSG00000141682	204285_s_at	*PMAIP1*	*Pmaip1*
ENSG00000141959	201102_s_at	*PFKL*	*Pfkl*
ENSG00000142178	208078_s_at	*SIK1*	*Sik1*
ENSG00000142230	1555618_s_at	*SAE1*	*Sae1*
ENSG00000142634	222483_at	*EFHD2*	*Efhd2*
ENSG00000142731	204886_at	*PLK4*	*Plk4*
ENSG00000143036	228221_at	*SLC44A3*	*Slc44a3*
ENSG00000143476	218585_s_at	*DTL*	*Dtl*
ENSG00000143479	210151_s_at	*DYRK3*	*Dyrk3*
ENSG00000144057	1555123_at	*ST6GAL2*	*St6gal2*
ENSG00000144136	201920_at	*SLC20A1*	*Slc20a1*
ENSG00000144369	227370_at	*FAM171B*	*Fam171b*
ENSG00000144554	242560_at	*FANCD2*	*Fancd2*
ENSG00000144567	222129_at	*FAM134A*	*Fam134a*
ENSG00000145050	202655_at	*MANF*	*Manf*
ENSG00000145386	213226_at	*CCNA2*	*Ccna2*
ENSG00000145476	226745_at	*CYP4V2*	*Cyp4v3*
ENSG00000145569	219694_at	*FAM105A*	*Fam105a*
ENSG00000145685	212658_at	*LHFPL2*	*Lhfpl2*
ENSG00000146038	222925_at	*DCDC2*	*Dcdc2a*
ENSG00000146267	232067_at	*C6orf168*	*Faxc*
ENSG00000146386	223361_at	*C6orf115*	*Abracl*
ENSG00000146674	210095_s_at	*IGFBP3*	*Igfbp3*
ENSG00000146950	204967_at	*SHROOM2*	*Shroom2*
ENSG00000147036	243856_at	*LANCL3*	*Lancl3*

Human ENSEMBL#	Probe on HU133+2.0	Human Gene Symbol	Mouse Gene Symbol
ENSG00000147416	201089_at	*ATP6V1B2*	*Atp6v1b2*
ENSG00000147509	210138_at	*RGS20*	*Rgs20*
ENSG00000147606	1552826_at	*SLC26A7*	*Slc26a7*
ENSG00000148154	224967_at	*UGCG*	*Ugcg*
ENSG00000148158	226249_at	*SNX30*	*Snx30*
ENSG00000148841	225582_at	*ITPRIP*	*Itprip*
ENSG00000148848	202952_s_at	*ADAM12*	*Adam12*
ENSG00000148926	202912_at	*ADM*	*Adm*
ENSG00000149483	223113_at	*TMEM138*	*Tmem138*
ENSG00000149485	208962_s_at	*FADS1*	*Fads1*
ENSG00000149554	205393_s_at	*CHEK1*	*Chek1*
ENSG00000149573	203780_at	*MPZL2*	*Mpzl2*
ENSG00000150510	230067_at	*FAM124A*	*Fam124a*
ENSG00000151239	201745_at	*TWF1*	*Twf1*
ENSG00000151491	202609_at	*EPS8*	*Eps8*
ENSG00000151725	218883_s_at	*MLF1IP*	*Mlf1ip*
ENSG00000152056	1555731_a_at	*AP1S3*	*Ap1s3*
ENSG00000153485	213246_at	*C14orf109*	*Tmem251*
ENSG00000153814	225800_at	*JAZF1*	*Jazf1*
ENSG00000154917	210127_at	*RAB6B*	*Rab6b*
ENSG00000155097	202874_s_at	*ATP6V1C1*	*Atp6v1c1*
ENSG00000155158	232000_at	*TTC39B*	*Ttc39b*
ENSG00000155307	220330_s_at	*SAMSN1*	*Samsn1*
ENSG00000155368	209389_x_at	*DBI*	*Dbi*
ENSG00000155886	229110_at	*SLC24A2*	*Slc24a2*
ENSG00000155897	206811_at	*ADCY8*	*Adcy8*
ENSG00000156802	235266_at	*ATAD2*	*Atad2*
ENSG00000156970	203755_at	*BUB1B*	*Bub1b*
ENSG00000157193	205282_at	*LRP8*	*Lrp8*
ENSG00000157456	202705_at	*CCNB2*	*Ccnb2*
ENSG00000157470	227756_at	*FAM81A*	*Fam81a*
ENSG00000157680	206806_at	*DGKI*	*Dgki*
ENSG00000158769	221664_s_at	*F11R*	*F11r*
ENSG00000158869	204232_at	*FCER1G*	*Fcer1g*
ENSG00000159167	204595_s_at	*STC1*	*Stc1*
ENSG00000159399	202934_at	*HK2*	*Hk2*
ENSG00000159842	212895_s_at	*ABR*	*Abr*
ENSG00000160271	209050_s_at	*RALGDS*	*Ralgds*
ENSG00000160714	217978_s_at	*UBE2Q1*	*Ube2q1*
ENSG00000161921	223454_at	*CXCL16*	*Cxcl16*
ENSG00000162066	219082_at	*AMDHD2*	*Amdhd2*
ENSG00000162341	229251_s_at	*TPCN2*	*Tpcn2*
ENSG00000162511	201721_s_at	*LAPTM5*	*Laptm5*
ENSG00000162704	211963_s_at	*ARPC5*	*Arpc5*
ENSG00000162772	1554420_at	*ATF3*	*Atf3*
ENSG00000162777	221081_s_at	*DENND2D*	*Dennd2d*

Human ENSEMBL#	Probe on HU133+2.0	Human Gene Symbol	Mouse Gene Symbol
ENSG00000163449	228981_at	*TMEM169*	*Tmem169*
ENSG00000163577	235296_at	*EIF5A2*	*Eif5a2*
ENSG00000163624	205709_s_at	*CDS1*	*Cds1*
ENSG00000163683	224990_at	*C4orf34*	*Smim14*
ENSG00000163686	45288_at	*ABHD6*	*Abhd6*
ENSG00000163694	218035_s_at	*RBM47*	*Rbm47*
ENSG00000163931	208700_s_at	*TKT*	*Tkt*
ENSG00000164054	222986_s_at	*SHISA5*	*Shisa5*
ENSG00000164124	228624_at	*TMEM144*	*Tmem144*
ENSG00000164181	227180_at	*ELOVL7*	*Elovl7*
ENSG00000164283	208394_x_at	*ESM1*	*Esm1*
ENSG00000164484	234994_at	*TMEM200A*	*Tmem200a*
ENSG00000164604	219898_at	*GPR85*	*Gpr85*
ENSG00000164713	223376_s_at	*BRI3*	*Bri3*
ENSG00000164733	200839_s_at	*CTSB*	*Ctsb*
ENSG00000164746	1557636_a_at	*C7orf57*	*Gm11992*
ENSG00000164877	219332_at	*MICALL2*	*Micall2*
ENSG00000164929	222780_s_at	*BAALC*	*Baalc*
ENSG00000164961	201985_at	*KIAA0196*	*E430025E21Rik*
ENSG00000165023	219619_at	*DIRAS2*	*Diras2*
ENSG00000165304	204825_at	*MELK*	*Melk*
ENSG00000165609	223100_s_at	*NUDT5*	*Nudt5*
ENSG00000165868	214434_at	*HSPA12A*	*Hspa12a*
ENSG00000166073	227846_at	*GPR176*	*Gpr176*
ENSG00000166165	200884_at	*CKB*	*Ckb*
ENSG00000166224	212322_at	*SGPL1*	*Sgpl1*
ENSG00000166228	203557_s_at	*PCBD1*	*Pcbd1*
ENSG00000166278	203052_at	*C2*	*C2*
ENSG00000166311	209420_s_at	*SMPD1*	*Smpd1*
ENSG00000166387	212841_s_at	*PPFIBP2*	*Ppfibp2*
ENSG00000166401	206034_at	*SERPINB8*	*Serpinb8*
ENSG00000166402	228882_at	*TUB*	*Tub*
ENSG00000166444	202440_s_at	*ST5*	*St5*
ENSG00000166546	214068_at	*BEAN1*	*Bean1*
ENSG00000166562	223299_at	*SEC11C*	*Sec11c*
ENSG00000166681	217963_s_at	*NGFRAP1*	*Ngfrap1*
ENSG00000166710	216231_s_at	*B2M*	*B2m*
ENSG00000166803	202503_s_at	*KIAA0101*	*2810417H13Rik*
ENSG00000166833	222599_s_at	*NAV2*	*Nav2*
ENSG00000166900	209238_at	*STX3*	*Stx3*
ENSG00000166908	218942_at	*PIP4K2C*	*Pip4k2c*
ENSG00000166927	223343_at	*MS4A7*	*Ms4a7*
ENSG00000167004	208612_at	*PDIA3*	*Pdia3*
ENSG00000167106	212400_at	*FAM102A*	*Fam102a*
ENSG00000167173	204494_s_at	*C15orf39*	*1700017B05Rik*
ENSG00000167460	209344_at	*TPM4*	*Tpm4*

Human ENSEMBL#	Probe on HU133+2.0	Human Gene Symbol	Mouse Gene Symbol
ENSG00000167535	209530_at	*CACNB3*	*Cacnb3*
ENSG00000167716	226738_at	*WDR81*	*Wdr81*
ENSG00000167900	1554408_a_at	*TK1*	*Tk1*
ENSG00000168038	232206_at	*ULK4*	*Ulk4*
ENSG00000168078	219148_at	*PBK*	*Pbk*
ENSG00000168135	208359_s_at	*KCNJ4*	*Kcnj4*
ENSG00000168234	1570552_at	*TTC39C*	*Ttc39c*
ENSG00000168374	201096_s_at	*ARF4*	*Arf4*
ENSG00000168398	205870_at	*BDKRB2*	*Bdkrb2*
ENSG00000168404	238025_at	*MLKL*	*Mlkl*
ENSG00000168461	217762_s_at	*RAB31*	*Rab31*
ENSG00000168490	205325_at	*PHYHIP*	*Phyhip*
ENSG00000168785	225388_at	*TSPAN5*	*Tspan5*
ENSG00000168917	219569_s_at	*TMEM22*	*Slc35g2*
ENSG00000169230	223032_x_at	*PRELID1*	*Prelid1*
ENSG00000169258	227975_at	*GPRIN1*	*Gprin1*
ENSG00000169299	223738_s_at	*PGM2*	*Pgm1*
ENSG00000169607	229610_at	*CKAP2L*	*Ckap2l*
ENSG00000169679	215509_s_at	*BUB1*	*Bub1*
ENSG00000169783	227933_at	*LINGO1*	*Lingo1*
ENSG00000170011	214156_at	*MYRIP*	*Myrip*
ENSG00000170266	201576_s_at	*GLB1*	*Glb1*
ENSG00000170312	210559_s_at	*CDK1*	*Cdk1*
ENSG00000170340	219326_s_at	*B3GNT2*	*B3gnt2*
ENSG00000170390	227666_at	*DCLK2*	*Dclk2*
ENSG00000170522	210868_s_at	*ELOVL6*	*Elovl6*
ENSG00000170540	211935_at	*ARL6IP1*	*Arl6ip1*
ENSG00000170579	206489_s_at	*DLGAP1*	*Dlgap1*
ENSG00000170915	227626_at	*PAQR8*	*Paqr8*
ENSG00000171189	207242_s_at	*GRIK1*	*Grik1*
ENSG00000171848	209773_s_at	*RRM2*	*Rrm2*
ENSG00000171951	204035_at	*SCG2*	*Scg2*
ENSG00000172071	218696_at	*EIF2AK3*	*Eif2ak3*
ENSG00000172548	230188_at	*NIPAL4*	*Nipal4*
ENSG00000172667	219628_at	*ZMAT3*	*Zmat3*
ENSG00000172725	64486_at	*CORO1B*	*Coro1b*
ENSG00000172817	207386_at	*CYP7B1*	*Cyp7b1*
ENSG00000172986	235733_at	*GXYLT2*	*Gxylt2*
ENSG00000173083	222881_at	*HPSE*	*Hpse*
ENSG00000173093	244833_at	*CCDC63*	*Ccdc63*
ENSG00000173821	225931_s_at	*RNF213*	*Rnf213*
ENSG00000174945	1562261_at	*AMZ1*	*Amz1*
ENSG00000175130	200644_at	*MARCKSL1*	*Marcksl1*
ENSG00000175175	236302_at	*PPM1E*	*Ppm1e*
ENSG00000175183	211126_s_at	*CSRP2*	*Csrp2*
ENSG00000175197	209383_at	*DDIT3*	*Ddit3*

Human ENSEMBL#	Probe on HU133+2.0	Human Gene Symbol	Mouse Gene Symbol
ENSG00000175274	214667_s_at	*TP53I11*	*Trp53i11*
ENSG00000175899	217757_at	*A2M*	*A2m*
ENSG00000176170	219257_s_at	*SPHK1*	*Sphk1*
ENSG00000176406	229823_at	*RIMS2*	*Rims2*
ENSG00000176771	239650_at	*NCKAP5*	*Nckap5*
ENSG00000176853	226294_x_at	*FAM91A1*	*D15Ertd621e*
ENSG00000176887	204915_s_at	*SOX11*	*Sox11*
ENSG00000176890	202589_at	*TYMS*	*Tyms*
ENSG00000176978	224814_at	*DPP7*	*Dpp7*
ENSG00000177425	204005_s_at	*PAWR*	*Pawr*
ENSG00000178718	223415_at	*RPP25*	*Rpp25*
ENSG00000178878	221031_s_at	*APOLD1*	*Apold1*
ENSG00000179051	224578_at	*RCC2*	*Rcc2*
ENSG00000179431	219522_at	*FJX1*	*Fjx1*
ENSG00000180537	230720_at	*RNF182*	*Rnf182*
ENSG00000181264	238497_at	*TMEM136*	*Tmem136*
ENSG00000181790	206083_at	*BAI1*	*Bai1*
ENSG00000182220	201444_s_at	*ATP6AP2*	*Atp6ap2*
ENSG00000182372	223912_s_at	*CLN8*	*Cln8*
ENSG00000182541	210582_s_at	*LIMK2*	*Limk2*
ENSG00000182612	223795_at	*TSPAN10*	*Tspan10*
ENSG00000182871	209081_s_at	*COL18A1*	*Col18a1*
ENSG00000182902	223605_at	*SLC25A18*	*Slc25a18*
ENSG00000183196	223786_at	*CHST6*	*Chst5*
ENSG00000183615	223657_at	*FAM167B*	*Fam167b*
ENSG00000183696	203234_at	*UPP1*	*Upp1*
ENSG00000183765	210416_s_at	*CHEK2*	*Chek2*
ENSG00000183856	229538_s_at	*IQGAP3*	*Iqgap3*
ENSG00000184117	201709_s_at	*NIPSNAP1*	*Nipsnap1*
ENSG00000184575	212160_at	*XPOT*	*Xpot*
ENSG00000184792	221237_s_at	*OSBP2*	*Osbp2*
ENSG00000184867	203404_at	*ARMCX2*	*Armcx2*
ENSG00000184992	231810_at	*BRI3BP*	*Bri3bp*
ENSG00000185222	217975_at	*WBP5*	*Wbp5*
ENSG00000185339	204043_at	*TCN2*	*Tcn2*
ENSG00000185340	31874_at	*GAS2L1*	*Gas2l1*
ENSG00000185480	227928_at	*C12orf48*	*Parpbp*
ENSG00000185518	205551_at	*SV2B*	*Sv2b*
ENSG00000185803	218151_x_at	*GPR172A*	*Slc52a2*
ENSG00000185896	201553_s_at	*LAMP1*	*Lamp1*
ENSG00000185950	209184_s_at	*IRS2*	*Irs2*
ENSG00000187164	221802_s_at	*KIAA1598*	*4930506M07Rik*
ENSG00000187210	205505_at	*GCNT1*	*Gcnt1*
ENSG00000187266	396_f_at	*EPOR*	*Epor*
ENSG00000187672	213938_at	*ERC2*	*Erc2*
ENSG00000188042	202208_s_at	*ARL4C*	*Arl4c*

Human ENSEMBL#	Probe on HU133+2.0	Human Gene Symbol	Mouse Gene Symbol
ENSG00000189067	200706_s_at	*LITAF*	*Litaf*
ENSG00000196136	202376_at	*SERPINA3*	*Serpina3n*
ENSG00000196208	205862_at	*GREB1*	*Greb1*
ENSG00000196405	227232_at	*EVL*	*Evl*
ENSG00000196526	203563_at	*AFAP1*	*Afap1*
ENSG00000196562	224724_at	*SULF2*	*Sulf2*
ENSG00000196576	208890_s_at	*PLXNB2*	*Plxnb2*
ENSG00000196935	233888_s_at	*SRGAP1*	*Srgap1*
ENSG00000196950	225295_at	*SLC39A10*	*Slc39a10*
ENSG00000197081	201393_s_at	*IGF2R*	*Igf2r*
ENSG00000197355	214755_at	*UAP1L1*	*Uap1l1*
ENSG00000197444	219277_s_at	*OGDHL*	*Ogdhl*
ENSG00000197535	227761_at	*MYO5A*	*Myo5a*
ENSG00000197629	226818_at	*MPEG1*	*Mpeg1*
ENSG00000197971	225407_at	*MBP*	*Mbp*
ENSG00000198648	202786_at	*STK39*	*Stk39*
ENSG00000198715	1558693_s_at	*C1orf85*	*0610031J06Rik*
ENSG00000198794	212699_at	*SCAMP5*	*Scamp5*
ENSG00000198805	201695_s_at	*PNP*	*Pnp*
ENSG00000198814	214681_at	*GK*	*Gyk*
ENSG00000198901	218009_s_at	*PRC1*	*Prc1*
ENSG00000204386	208926_at	*NEU1*	*Neu1*
ENSG00000204681	205890_s_at	*GABBR1*	*Gabbr1*
ENSG00000205060	238418_at	*SLC35B4*	*Slc35b4*
ENSG00000205208	235088_at	*C4orf46*	*4930579G24Rik*
ENSG00000205336	212070_at	*GPR56*	*Gpr56*
ENSG00000213186	227801_at	*TRIM59*	*Trim59*
ENSG00000213614	201765_s_at	*HEXA*	*Hexa*
ENSG00000213719	208659_at	*CLIC1*	*Clic1*
ENSG00000216490	201422_at	*IFI30*	*Ifi30*
ENSG00000219438	237094_at	*FAM19A5*	*Fam19a5*
ENSG00000225190	212717_at	*PLEKHM1*	*Plekhm1*
ENSG00000241973	213408_s_at	*PI4KA*	*Pi4ka*
ENSG00000243649	202357_s_at	*CFB*	*Gm20547*
ENSG00000244607	1554023_s_at	*CCDC13*	*Ccdc13*
ENSG00000247746	237247_at	*USP51*	*Usp51*
ENSG00000248905	238621_at	*FMN1*	*Fmn1*
ENSG00000249481	239870_at	*SPATS1*	*Spats1*

Supplemental Experimental Procedures

Mice

All mouse work was performed with the approval of the institutional animal care and use committee and in accordance with international legal and ethical norms. The *EWSR1-ATF1*, *SS18-SSX2*, and *LacZ* mice were previously described (Haldar et al., 2007; Soriano, 1999; Straessler et al., 2013), as were *Rosa26-CreER* and *Prx1-CreERT2* mice (Badea et al., 2003; Hasson et al., 2007). The full length cDNA of type 2 *ASPSCR1-TFE3* was reverse transcribed from total RNA isolated from a human ASPS. The *Rosa26-LSL-AT3* targeting vector was electroporated into R1 mouse embryonic stem cells. Clones were screened by long range PCR (CCT AAA GAA GAG GCT GTG CTT TGG and CAG TAG TCC AGG GTT TCC TTG ATG; GTG CAG TGT TGA GGG CAA TCT G and TAT GGC TTC TGA GGC GGA AAG A), then subjected to Southern blot analysis. Cells from a targeted clone were microinjected into C57BL/6 blastocysts. Resulting chimeras were mated to C57BL/6 mice and their offspring genotyped by long-range PCR.

Subsequent generations were PCR genotyped using tail-tip DNA: Forward – GTT ATC AGT AAG GGA GCT GCA GTG G, Reverse targeted – AAG ACC GCG AAG AGT TTG TCC TC, Reverse wild-type – GGC GGA TCA CAA GCA ATA ATA ACC. 30 cycles of 95°C for 30 seconds, 59°C for 45 seconds and 72°C for 30 seconds yield a 300bp band from the targeted locus and a 415bp band from the wild-type locus.

UU IR Author Manuscript

Imaging

Radiographs were obtained using a Kodak Carestream 4000 Pro Fx (Carestream Health, Inc., Rochester, NY, USA). Gross images were obtained with a Leica AF6000 (Leica Microsystems, Wetzlar, Germany) and photomicrographs with an Olympus BX43 scope and DP26 camera (Olympus America, Center Valley, PA, USA).

Histology

Tissues were harvested post-mortem, fixed in 10% buffered formalin overnight, embedded in paraffin following serial dehydration in ethanol, sectioned at 4µm and stained with H&E. dPAS utilized a 45 minute digestion with diastase solution (ARUP, Salt Lake City, UT, USA) at 37°C, rinsing, staining in Schiff reagent (ARUP) for 30 minutes, rinsing, and hematoxylin counterstaining. Immunohistochemistries following 1-hour pH8.0 cell conditioning 1 (Ventana Medical Systems, Tuscon, AZ, USA) antigen retrieval, proceeded for human TFE3 (Cell Marque, clone MRQ-37, rabbit polyclonal, 1:100 dilution for 2 hours at 37°C), Cd31 (Abcam, rabbit polyclonal, 1:25 dilution for 2 hours at 37°C), and Ki-67 (Abcam, rabbit polyclonal, 1:250 dilution for 2 hours at room temperature) using the BenchMark Ultra automated immunostainer (Ventana Medical Systems) with a biotinylated secondary antibody, DAB detection (IView) and hematoxylin counterstain.

For assessment of hypoxia, *Rosa26*$^{LSL\text{-}AT3}$/$_{CreER}$ mice received IP 60mg/kg pimonidazole 90 minutes prior to euthanasia. Tumors, skin, kidney, brain, and liver were rapidly collected and fixed in 10% formalin at 4°C overnight, serially dehydrated, embedded in paraffin, and sectioned at 4µm. Immunohistochemistry using antibodies

against mouse Hif1α (Novus Biologicals, H1alpha67 clone, dilution 1:500 for overnight at room temperature) or pimonidazole-thiol adducts (Hypoxyprobe monoclonal antibody, 1:50 dilution for 1 hour at room temperature) was performed following 20 minute heat antigen retrieval and using IgG-horse radish peroxidase goat anti-rabbit secondary (1:250 dilution, 1 hour at room temperature) with DAB detection and hematoxylin counterstain.

For X-gal staining, mice received IP 20mg/kg tamoxifen (Sigma-Aldrich, St. Louis, MO, USA) on days 14, 16, and 18 of life. Cranium and limbs harvested on day 21 were fixed for 1 hour in 4% paraformaldehyde, decalcified for 2 weeks in pH7.4 14% ethylenediaminetetracetic acid at 4°C, dehydrated in glucose gradients, and embedded in OCT (Sakura Finetek, Torrance, CA, USA). 8µm-thick mid-sagittal sections of the cranium or shoulder were fixed with glyceraldehyde 0.25% for 10 minutes, washed thrice, and then incubated at 37°C for 8 hours in Xgal 1mg/mL with 30 mM potassium ferricyanide, 30 mM potassium ferrocyanide, 0.01% sodium deoxycholate, 0.02% Nonidet P-40 and 1 mM MgCl2. After rinsing in saline and distilled water, they were counterstained in nuclear fast red (Sigma).

Tissue lactate measurement

Tissues were harvested at 2 months from 5 wild-type mice, snap frozen in liquid nitrogen, weighed, homogenized into 4.2% perchloric acid (ARUP) at 4°C, and centrifuged. 150uL of the supernatant was added to 900uL of a solution of 0.4M hydrazine (Fisher, Pittsburgh, PA, USA) and 0.5M glycine (Fisher) buffered by ethylenediamine tetra-acetic acid (Fisher) and brought to pH9.0 with sodium hydroxide

UU IR Author Manuscript

(Fisher), with 14 units/mL L-lactate dehydrogenase from bovine heart (Sigma) and 1.83mg/mL oxidized nicotinamide adenine dinucleotide (Fisher). Reactions were incubated at 35°C in parallel with triplicate reactions using lithium lactate concentration standards in 0.05% sulfuric acid. Absorbance at 340nm was measured with a Spectramax M5e (Molecular Devices Corporation, Sunnyvale, CA, USA) plate reader, lactate concentrations calculated for each sample from the standard curve, and normalized by the input tissue mass to generate tissue lactate concentrations. Reactions and standards were repeated for confirmation.

Clinical

With the approval of the institutional review board and in accordance with all international legal and ethical standards, fresh surgical specimens from consenting patients were placed in RNA-Later (Invitrogen) at 4°C overnight prior to long term storage at -80°C. Cases were annotated with histopathology, molecular, and clinical data. 5 ASPS cases and 3 uninvolved quadriceps samples were analyzed.

Transcriptome analysis

Total RNA was isolated using the RNeasy mini kit (Qiagen, Valencia, CA, USA). For sequencing, RNA was prepared using an Illumina TruSeq RNA kit (Illumina, Inc., San Diego, California) and checked with an Agilent Bioanalyzer RNA 6000 chip (Agilent Technologies, Santa Clara, California). mRNAs were captured using the Ribo-Zero method (Illumina) and fragmented. Library quality was then checked by Nanodrop analysis (Thermo Scientific, Wilmington, Delaware), qPCR quantitation using Illumina

UU IR Author Manuscript

primers, and another bioanalyzer run. Sequencing was performed on an Illumina HiSeq 2000 (Illumina) using a 50 cycle single end read. PhiX control library reads were added to each lane for quality assurance. Reads were aligned to the mm10 mouse or the hg19 human genome builds. The OverdispersedRegionScanSeqs script in the USeq package (Nix et al., 2008) calculated the expression levels of ENSEMBL genes in FPKM values. USeq also discovers differentially expressed genes between two RNA-seq libraries by calling the DESeq R package (Anders and Huber, 2010). Internally, the DESeq algorithm uses a negative binomial distribution to model the read coverage, which is robust to the between-libraries variations of RNA-seq data by using biological replicate data.

GEO data were normalized by DChip (Li and Hung Wong, 2001). GSEA was performed with Broad Institute software (Mootha et al., 2003; Subramanian et al., 2005). The Harris hypoxia gene set is curated by the Broad Institute (Harris, 2002), as is MitoCarta, including the original 1098 mouse genes, whose proteins localize to the mitochondria, and their 1013 human homologues (Pagliarini et al., 2008). Gene ontology analysis was performed with GO-Elite software (Zambon et al., 2012).

Tissue Culture

The ASPS-1 cell line was cultured in Dulbecco's Modified Eagle Medium with F12 Glutamax (DMEM/F12 from Life Technologies) with 10% fetal bovine serum (FBS from Life Technologies). The FU-UR-1 cell line was cultured in DMEM/F12+15%FBS. For tissue culture, CHC (Sigma) was dissolved as a 1.5M solution in DMSO and sodium lactate (Sigma) as a 2M solution in culture medium. Proliferation assays were initiated

as 5000 cells seeded into each 96-well plate well, with lactate added 24 hours later. CellTiter-Glo (Promega) assay, applied using manufacturer's recommended protocol, determined relative viability on a Perkin-Elmer Envision 2104 multilabel reader at 48 hours for the faster growing FU-UR-1 cells and 72 hours for the slower growing ASPS-1 cells. For Westerns, plates were quickly chilled, the media aspirated and replaced with 4°C PBS, and cells collected by scraping and centrifuged to remove excess PBS. The NE-PER Nuclear and Cytoplasmic Extraction assay (Pierce) was then used according to the recommended protocol to isolate the nuclear and cytoplasmic fractions of total protein. After running and transferring to nitrocellulose, the membrane was divided for an overnight GAPDH control and HIF1α experimental antibody (Novus Biologicals) after blocking for an hour in 5% milk. Imaging used a Bio-Rad ChemiDoc MP system.

Metabolic phenotyping

Tissue sections obtained immediately post mortem from tumors in mice of each genotype were placed in microwells per the manufacturer's instructions for assessment on the Seahorse XF24 (Seahorse Bioscience, Massachusetts, USA). Minimal initial media included 2mM glucose in DMEM. An injection of 10mM sodium lactate was timed and the subsequent oxygen consumption rate measured 24 minutes later.

***Lactate administration* in vivo**

Isotonic sterile sodium lactate (Sigma) or sodium chloride (Sigma) was administered IP daily to $Rosa26^{LSL\text{-}AT3}/_{CreER}$ mice randomized to either treatment after a tumor was noted.

UU IR Author Manuscript